were resistant to HFD-induced obesity and hepatic steatosis. The liver of HFD-fed FS I-I Tg mice showed significantly different fatty acid composition compared with that seen in the control mice. Our studies suggest that follistatin-derived myostatin inhibitors offer a therapeutic option for obesity, diabetes, and hepatic steatosis.

MATERIALS AND METHODS

Animals. The establishment of skeletal muscle-specific FS I-I Tg mice is described in our previous paper (27). In brief, *Eco*RI-*Sma*I fragment covering the whole coding sequence of FS I-I was subcloned into the MDAF2 vector containing the myosin light-chain promoter SV40 processing sites and MLC1/3 enhancer. *Cla*I fragment with 3.9 kb was microinjected to produce FS I-I transgenic mice (27). The transgene was expressed in skeletal muscles but not in cardiac muscle or adipose tissues. FS I-I Tg male mice and wild-type littermates were obtained from the offspring of FS I-I Tg mice mated with C57BL/6 mice. The genotypes were determined by PCR as previously described (27). The FS I-I Tg and littermate male mice were weaned at 4 wk of age and given free access to either a normal-fat (NFD; 5% kcal fat; CE-2; CLEA, Shizuoka, Japan) or a high-fat diet (HFD; 32% kcal fat, High Fat Diet 32, CLEA) from 4 to 13 wk. Food intake did not differ between the two genotypes on the HFD. Body weight was recorded every week. All mice were housed in cages with a constant temperature (22°C) and a 12:12-h light-dark cycle. All experiments were performed at the Laboratory Animal Center with approval from the Animal Research Committee at Fujita Health University.

Analysis of adipose tissue, skeletal muscle, and liver. Adipose tissues (retroperitoneal, epididymal, and inguinal fat pads), skeletal muscles [tibialis anterior (TA), extensor digitorum longus (EDL), quadriceps femoris (Qf), and soleus], and liver samples were obtained from mice at 13 or 20 wk of age. Adipose tissue and muscles were also obtained from NFD- and HFD-fed mice at *week 13*. The wet tissue weights were measured.

Histological analyses of adipose tissues and liver. The adipose tissues and livers either from FS I-I Tg mice or littermates were fixed in 4% paraformaldehyde (PFA), dehydrated in ethanol, embedded in paraffin, and sectioned at a thickness of 6 μm. The sections were then deparaffinized, rehydrated, and stained with hematoxylin and eosin (H&E). The area of adipocytes was determined in images stained with H&E. The area of 200 adipocytes per mouse was determined in five wild-type and five FSI-I Tg mice (1,000 adipocytes for each genotype), and the average cell area was determined. Morphometric analyses to measure adipocyte area and size were performed using WinROOF software (Mitani, Fukui, Japan).

Electron microscope analysis. Adipose tissue samples were fixed for 4 h with 2% PFA and 2.5% glutaraldehyde in phosphate-buffered saline (PBS) at room temperature. The specimens were then postfixed at room temperature for 1 h with 2% osmium tetroxide in Millonig's buffer containing 0.54% glucose and dehydrated through an ethanol gradient. For scanning electron microscopy, the dehydrated specimens were then immersed in *t*-butyl alcohol, dried using a freeze-drying device, coated with gold using an ion sputtering device (JEE-420T, JEOL), and examined under a scanning electron microscope (H7650; Hitachi, Tokyo, Japan). For transmission electron microscopy, specimens were immersed in QY-1 (Nisshin EM, Tokyo, Japan), embedded in epoxy resin (Epon812; Polyscience, Wako Pure Chemical Industries, Osaka, Japan), and cut into ultrathin sections. The sections were stained with uranyl acetate and lead citrate, followed by transmission electron microscopy at an accelerating voltage of 80 kV (JEM-1010TEM, JEOL). One hundred fifty mitochondria of epididymal adpipocytes each from three wild-type and FS I-I Tg mice were analyzed using WinROOF software.

Quantitative real-time PCR. The relative expressions of uncoupling protein-3 (UCP3), acetyl-CoA carboxylase-1 (ACC1), stearoyl-CoA desaturase-1 (SCD1), glucokinase (Gck), and phosphofructokinase (PFK) were determined by quantitative (q)PCR using a TAKARA Thermal Cycler Dice Real-Time System (Takara Bio, Shiga, Japan). Briefly, mRNA was isolated from liver and adipose tissues from FS I-I Tg mice and wild-type littermates by use of TRIzol (Invitrogen, Tokyo, Japan) with standard techniques. The isolated RNA was cleaned by DNaseI and purified using RNeasy Tissue kits (Qiagen, Tokyo, Japan). Reverse transcription was carried out with 500 ng of RNA using QuantiTect reverse transcription kits (Qiagen) according to the manufacturer's instructions.

We used Primer 3 software to design the primers for UCP3 (forward: 5′-CCGGTGGATGTGGTAAAGAC-3, reverse: 5′-AAGCTCCCAGACGCAGAAAG-3); ACC1 (forward: 5′-CCCATCCAAACAGAGGGAAC-3, reverse: 5-CTGACAAGGTGGCGTGAAG-3); SCD1 (forward: 5′-CAAGCTGGAGTACGTCTGGA-3′, reverse: 5′-CAGAGCGCTGGTCATGTAGT-3′); Gck (forward: 5′-TGGGCTTCACCTTCTCCTTC-3′, reverse: 5′-CGATGTTGTTCCCTTCTGCT-3′); and PFK (forward: 5′-GAAGCCAATCACCTCAGAAGAC-3′, reverse: 5′-TTCCACACCCATCCTGCT-3′). Each well of the 96-well reaction plate contained a total volume of 25 μl. cDNA (0.5 μl) solution was combined with each of forward and reverse primers (10 μM), distilled water, and SYBR Premix Ex Taq (Takara Bio). All reactions were performed in triplicate. The relative amounts of RNAs were calculated using the comparative C_T method. We used hepatic glyceraldehyde-3-phosphate dehydrogenase (GAPDH) and adipose tissue 36B4 as controls. Significant differences between the wild-type and FS I-I Tg mice were analyzed by Student's *t*-test.

Western blotting. Adipose tissues (epididymal and inguinal fat pads), skeletal muscle (Qf), and liver were dissected from wild-type and FSI-I Tg mice. Samples were homogenized in a buffer containing 50 mM Tris·HCl, pH 7.5, 150 mM NaCl, 5 mM NaF, 1% Nonidet P-40, 5 mM β-glycerophosphate, 1 mM phenylmethylsulfonyl fluoride, 4 μg/ml leupeptin, and 1 μg/ml aprotinin and centrifuged at 15,000 rpm for 10 min at 4°C, and the lipid-free lysates were collected. Aliquots of the lysates containing 30 μg of protein or serum containing 60 μg of protein were separated by sodium dodecyl sulfate-polyacrylamide gel electrophoresis and transferred onto polyvinylidene difluoride membranes. The membrane was blocked in 5% skim milk for 1 h at room temperature. The membranes were then probed with anti-cytochrome *c*, phosphorylated Smad 3, or Smad 3 (Cell Signaling Technology, Beverly, MA) at 4°C overnight (1:1,000 dilution), followed by incubation with horseradish peroxidase-conjugated secondary antibodies and chemiluminescence reactions by ECL plus (GE Healthcare, Tokyo, Japan). As a loading control, antibodies to tubulin or actin (Cell Signaling Technology, Beverly, MA) were used. Detection of FS I-I or follistatin by Western blotting was performed using rabbit polyclonal antibodies (ABPIII) raised against follistatin domain I of follistatin (31). Images of the developed immunoblots were captured using a cooled CCD camera system (Light-Capture; ATTO, Tokyo, Japan).

Measurement of serum parameters and triglycerides. Wild-type and FS I-I Tg mice (n = 4–6 per group) fed the NFD or HFD from *weeks 4* to *13* of age were fasted overnight at *week 13* for 16 h before blood sampling. The triglyceride, nonesterified fatty acid (NEFA), cholesterol, fasting glucose, insulin, leptin, and adiponectin concentrations were measured in serum samples prepared from whole blood collected from the retroorbital venous plexus of anesthetized mice. Plasma, total cholesterol, and NEFA were measured using enzymatic assays (triglyceride E, cholesterol E, and NEFA tests, respectively; Wako Pure Chemical Industries, Osaka, Japan). Plasma leptin, adiponectin, and insulin levels were measured using enzyme-linked immunoassays from Morinaga (Kanagawa, Japan), R&D systems (Gunma, Japan), and Otsuka (Tokyo, Japan), respectively. Triglycerides from liver and skeletal muscle were extracted with chloroform-methanol (2:1, vol/vol), centrifuged twice to remove debris, dried, and resuspended in 2-propanol containing 10% Triton X-100 (17). Triglyceride contents were enzymatically measured using a triglyceride E test. Mouse preadipocyte 3T3-L1 cells and human hepatocyte Hep

G2 cells were grown in Dulbecco's modified Eagle's medium (DMEM) supplemented with 10% fetal calf serum. Cells (1×10^5)/12-well plates of differentiating 3T3-L1 cells were stimulated with either 80 ng/ml FS I-I or 40 ng/ml myostatin (R&D systems) for 3 days. Hep G2 cells treated with 3 mg/ml glucose, 10 μg/ml insulin, and either 80 ng/ml FS I-I or 40 ng/ml myostatin for 3 days. Cellular triglycerides were extracted and measured as described above. All assays were performed according to the manufacturer's protocol.

Glucose tolerance test. Glucose tolerance tests were performed in six to eight mice per group at 13 wk of age after being fed the NFD or HFD for 9 wk. The mice were fasted overnight and then received an intraperitoneal injection of 10% dextrose (1 g/kg body wt). Blood was collected from the tail at 0, 15, 30, 60, and 120 min after dextrose injection, and blood glucose was measured using an Accu-Check glucose monitor (Roche Diagnostic, Indianapolis, IN).

Insulin tolerance test. Insulin tolerance tests were performed in five mice per group at 13 wk of age after being fed the HFD for 9 wk. The mice were starved for 16 h and received an intraperitoneal injection of human insulin (0.75 U/kg body wt; Sigma-Aldrich Japan). Blood glucose was measured at 0, 30, 60, and 90 min after injection using an Accu-Check glucose monitor (24).

Measurement of hepatic fatty acid content. Approximately 100 mg of liver tissue was obtained from wild-type and FS I-I Tg mice fed the NFD or HFD for 9 wk ($n = 6$ per group). Lipids were extracted using the Bligh-Dyer chloroform-methanol method (4). The extracted lipids were dissolved in 1 ml of chloroform and subjected to methanolysis-gas chromatographic analysis (3). Methyl stearate was used to generate a standard curve for quantitation. The determinations were repeated at least twice, and essentially the same results were obtained.

Metabolic rate analysis. Oxygen consumption was measured with an indirect calorimetric metabolism measuring system (model MK-5000RQ, Muromachikikai) (17). Each mouse was kept in a sealed chamber with an air flow of 0.6 l/min for 2 h during the light cycle. Air was sampled every 3 min, and the consumed oxygen concentration ($\dot{V}O_2$) was calculated (24). Five mice each for wild-type and FS I-I Tg mice fed NMD were analyzed.

Statistical analysis. Results are presented as means ± SD. Statistical significance was assessed by Student's *t*-tests. Differences between groups were considered statistically significant at $P < 0.05$. *P* values are presented in figure and table legends.

RESULTS

Decreased fat accumulation in FS I-I tg mice. We previously reported (27) that FS I-I Tg mice show a marked increase in skeletal muscle mass compared with wild-type mice when fed a NFD. Intriguingly, even with a NFD, FS I-I Tg mice showed age-dependent decreased fat accumulation. Although there was no difference in individual fat pad weights between wild-type and FS I-I Tg mice at 13 wk of age (data not shown), there was a significant difference at 20 wk of age. For example, at 20 wk of age, the weight of the epididymal fat pad was 60% lower in FS I-I Tg mice than in wild-type mice (Fig. 1*A*). Furthermore, the weights of the inguinal and retroperitoneal fat pads of FS I-I Tg mice were 33 and 67% lower, respectively, in FS I-I Tg mice than in wild-type mice. Therefore, we quantified the adipocyte size histologically using H&E staining (Fig. 1*B*)

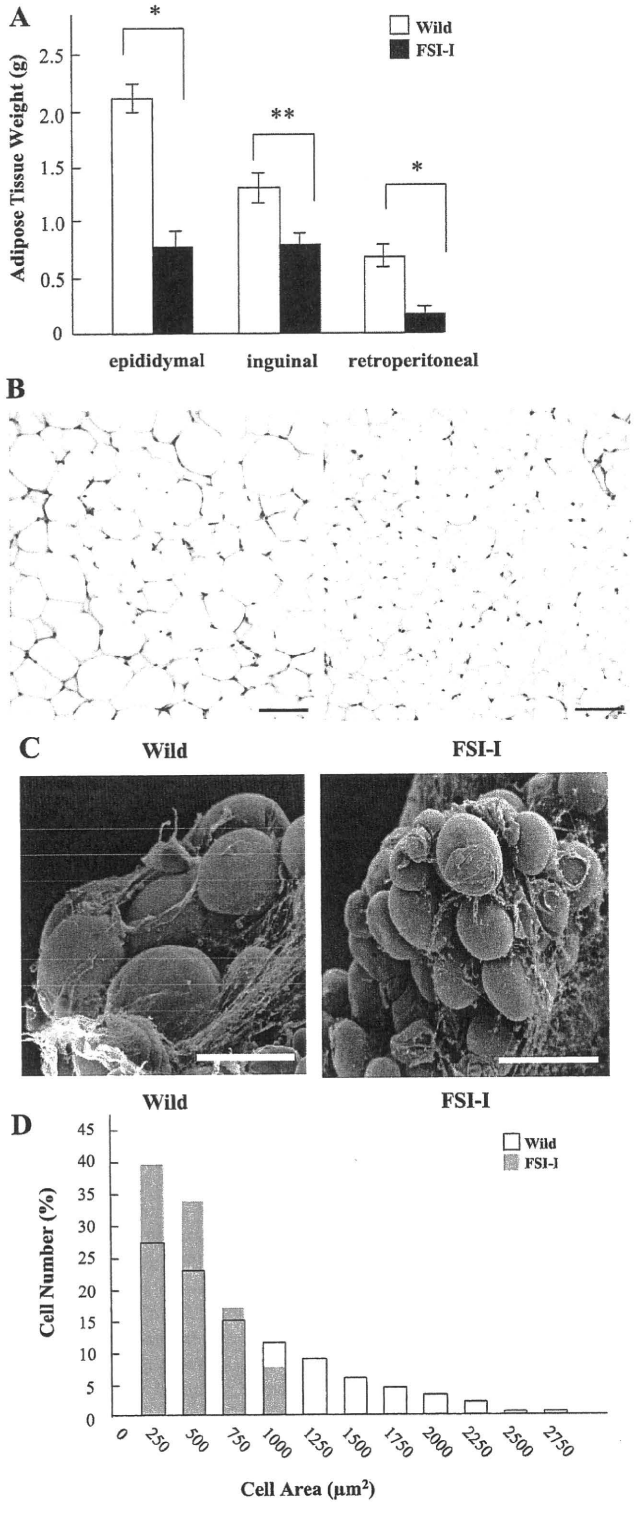

Fig. 1. *A*: adipose tissue weights (g) of 20-wk-old male wild-type and transgenic (Tg) mice with a myostatin inhibitor derived from follistatin [follistatin (FS)-derived peptide (FS I-I)] fed a control diet. Epididymal, inguinal, and retroperitoneal fat pads from 5 mice each from wild-type and FSI-I Tg mice were dissected and weighed. $^*P < 0.005$ and $^{**}P < 0.03$, Student's *t*-test. *B*: histological analysis of adipose tissues. Epididymal fat pads from 20-wk-old wild-type and FS I-I Tg mice were sectioned and stained with H&E. Scale bar, 100 μm. *C*: scanning electron microscopy of epididymal fat pads. 20-wk-old wild-type (*left*) and FS I-I Tg mice (*right*) were analyzed. Scale bar, 120 μm. *D*: distribution of epididymal adipocyte area in 20-wk-old wild-type and FS I-I Tg mice; 200 adipocytes were counted per mouse (5 mice per group). The percentage of adipocytes with indicated areas per total adipocytes was calculated and plotted. The mean adipocyte area was smaller in FS I-I Tg mice (717.4 ± 579.1 μm^2) than in wild-type mice (436.8 ± 309.1 μm^2).

and by scanning electron microscopy (Fig. 1*C*). Both techniques confirmed that adipocyte size was smaller in FS I-I Tg mice than in wild-type mice. Therefore, we determined the mean adipocyte area. Quantification of the area of individual adipocytes is shown in Fig. 1*D*. At *week 20* of age, the mean adipocyte area was smaller in FS I-I Tg mice than in wild-type mice (436.8 ± 309.1 vs. 717.4 ± 579.1 μm^2, respectively; Fig. 1*D*). These results indicate that FS

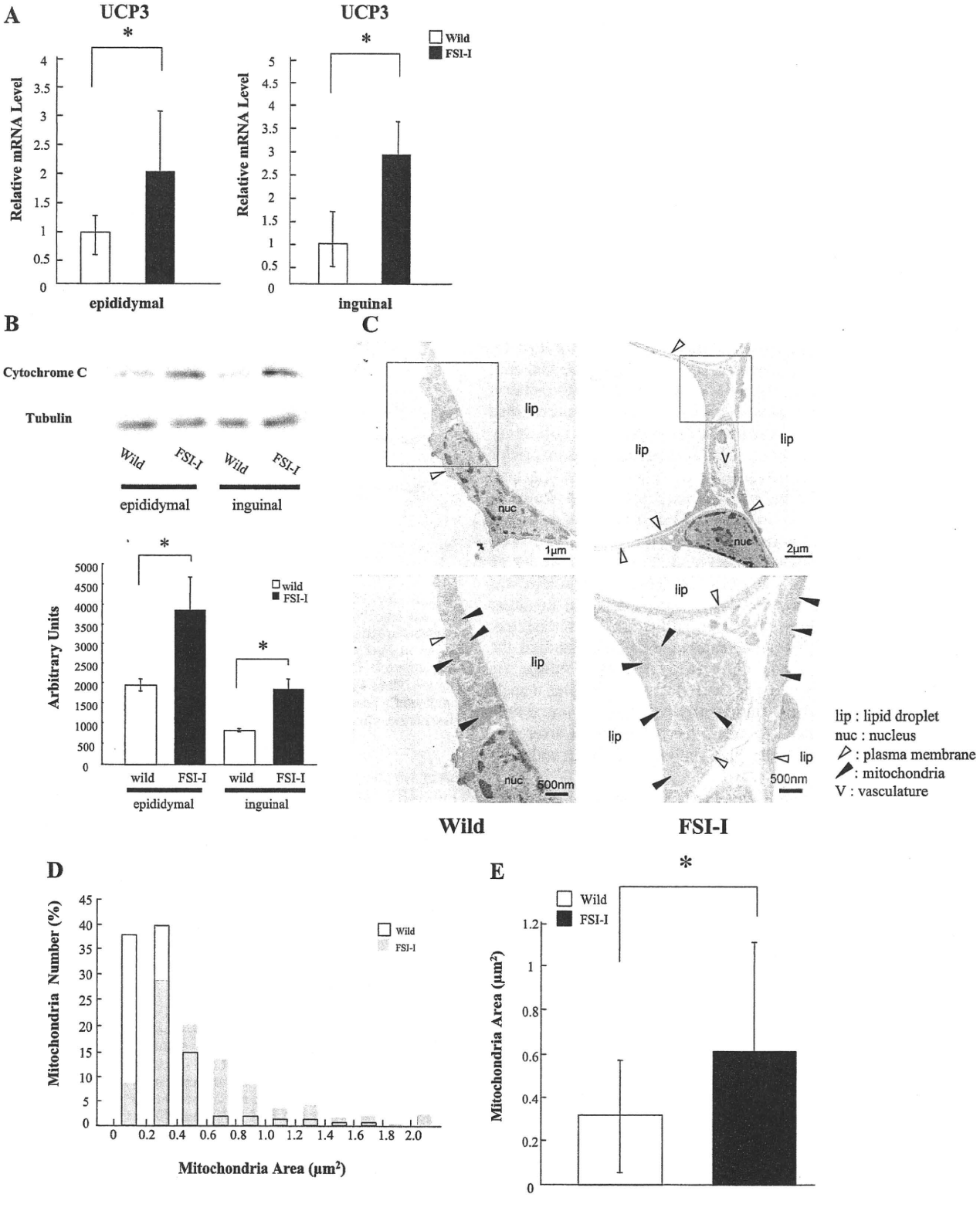

I-I Tg mice showed less fat accumulation than wild-type mice when fed a NFD.

Changes in expression of metabolic molecules in FS I-I Tg mice. We examined the expression levels of mRNAs encoding the UCPs, proteins expressed on the inner membrane of the mitochondria that uncouple the proton gradient from ATP synthesis and are implicated in thermogenesis (7). The expression levels of UCP3 in epididymal and inguinal adipose tissues were increased two- and threefold, respectively, in FS I-I Tg mice compared with wild-type mice (Fig. 2*A*). However, the expression levels of UCP1 and UCP2 mRNAs in adipose tissues in FS I-I Tg mice and wild-type mice were comparable (data not shown).

We next quantified the abundance of mitochondria in adipose tissues by using the mitochondria marker cytochrome *c* (Fig. 2*B*). Consistent with the increase in UCP3 mRNA, the protein expression of cytochrome *c* was increased in the epididymal and inguinal fat pads in FS I-I Tg mice compared with wild-type mice (Fig. 2*B*). In skeletal muscle, cytochrome expression did not change (Suppl. Fig. S1; supplementary materials are found with the online version of this paper on the Journal website). We also determined mitochondria size by transmission electron microscopy (Figs. 2, *C* and *D*, and S2), which revealed that both the number and size of mitochondria in adipocytes were increased in FS I-I Tg mice compared with wild-type mice. These results raise the interesting possibility that FS I-I Tg mice exhibit increased energy metabolism and/or energy partitioning between adipose tissue and skeletal muscle.

Expression of FS I-I and altered Smad 3 phosphorylation in FS I-I Tg mice. To ascertain that FS I-I expression is restricted in skeletal muscle, we performed Western blotting using skeletal muscle, liver, adipose tissues and serum from wild-type and FS I-I Tg mice. As shown in Fig. 3*A*, FS I-I protein was expressed in skeletal muscle, but was not detected in either liver or adipose tissues. In serum, follistatin was detected, whereas FS I-I was hardly detectable. Next, we studied the phosphorylation of Smad 3 protein by immunoblotting. As shown in Fig. 3*B*, Smad 3 phosphorylation in skeletal muscle from FS I-I Tg mice was significantly reduced compared with that from control mice. In other tissues such as liver and adipose tissues, Smad 3 phosphorylation was either undetectable or unchanged.

FS I-I Tg mice are resistant to HFD-induced obesity. We previously reported that NFD-fed FS I-I Tg mice exhibited greater weight gain than wild-type mice between 6 and 15 wk of age, even though food intakes were comparable (27). Here, the FS I-I Tg and wild-type mice were fed a HFD from *weeks 4* to *13* of age to induce obesity. Interestingly, weight gain did not differ between FS I-I Tg and wild-type mice (Fig. 4*A*). However, the weight of adipose tissue depots was lower in FS I-I Tg mice than in wild-type mice, being 25.0 and 34.3% lower for the inguinal and retroperitoneal fat pads, respectively (Fig. 4*B*). By contrast, FS I-I Tg mice exhibited increased muscle weight, as the TA, EDL, Qf, and soleus muscles were 43, 45, 21, and 27% higher in FS I-I Tg mice than in wild-type mice (Fig. 4*C*). Thus, the absence of a difference in body weight gain between wild-type mice and FS I-I Tg mice fed the HFD was attributed to changes of adipose tissue, muscle, and liver weights in FS I-I Tg mice (see Figs. 4, *B* and *C*, and 5*B*).

We next measured serum parameters, including triglyceride, NEFA, total cholesterol, insulin, leptin, and adiponectin levels

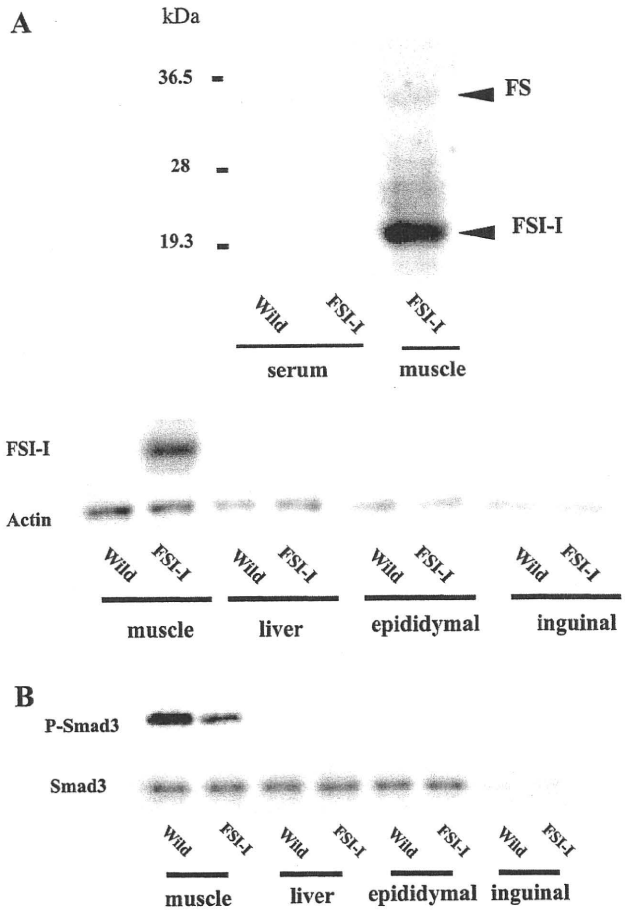

Fig. 3. *A*: detection of FS and FS I-I in serum, femoris skeletal muscle (Qf), liver, and fats. FS is detected as 33-kDa protein in serum, whereas FS I-I is not detectable in serum in FS I-I Tg mice (*top*). FS I-I is detected in skeletal muscle but not in liver or fats (*bottom*). *B*: detection of phosphorylated Smad3 in skeletal muscle, liver, and epididymal and inguinal fats. In quadriceps skeletal muscle (Qf) of FS I-I Tg mice, phosphorylated Smad 3 is reduced compared with that of wild-type mice. Smad 3 antibody was used as a loading control. In other tissues, phosphorylation of Smad 3 is either undetectable or unchanged.

Fig. 2. *A*: relative mRNA expression of UCP3 in epididymal and inguinal adipose tissues in wild-type and FS I-I Tg mice. Adipose tissues from 5 mice each for wild-type and FS I-I Tg mice were used and quantitated. UCP3 mRNA expression levels were quantified by RT-PCR. $*P < 0.05$, Student's *t*-test. *B*: protein expression of cytochrome *c* in epididymal and inguinal fat pads from wild-type and FS I-I Tg mice. Cytochrome *c* was detected at 14 kDa. Tubulin expression was used as a loading control (*top*). Adipose tissues from 3 mice each for wild-type and FS I-I Tg mice were used and quantitated. $*P < 0.02$, Student's *t*-test (*bottom*). *C*: transmission electron microscopy of epididymal adipose tissues from 20-wk-old wild-type and FS I-I Tg mice. Higher magnification views of indicated regions (squares) at *top* are shown at *bottom*. Scale bars, 1 μm in *top left*, 2 μm in *top right*, and 500 nm in *bottom*. Lip, lipid droplet; nuc, nucleus; white arrowheads, plasma membranes; black arrowheads, mitochondria; V, vasculature. *D*: analysis of mitochondria size and number from wild-type and FS I-I Tg mice. One hundred fifty mitochondria of epididymal adipocytes each from 3 wild-type and FS I-I Tg mice were analyzed and plotted. *E*: mean mitochondria areas of wild-type and FS I-I Tg mice. $*P < 0.001$, Student's *t*-test.

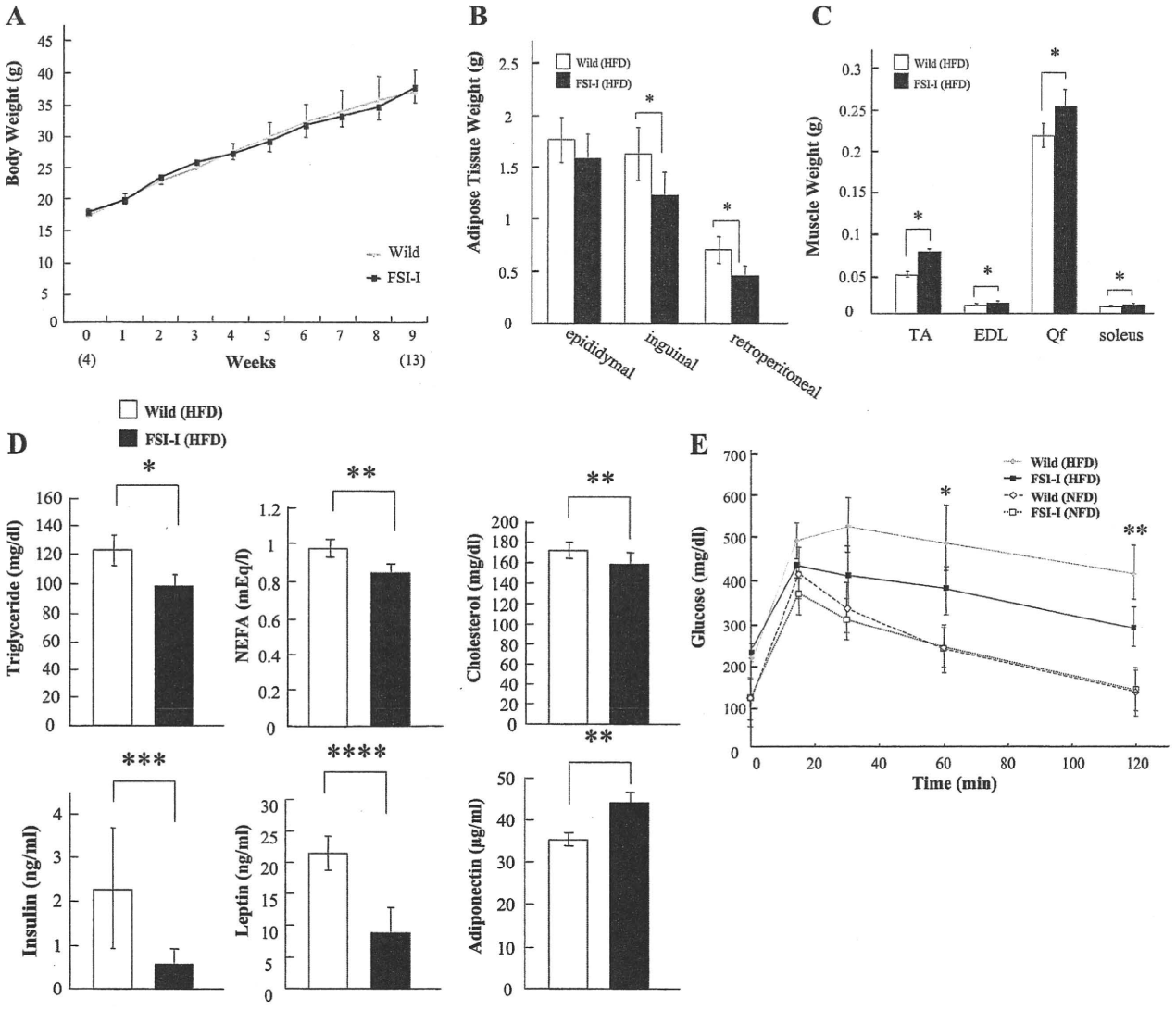

Fig. 4. *A*: body weights (g) of wild-type and FS I-I Tg mice fed a high-fat diet (HFD) from 4 to 13 wk of age; $n = 5$ mice per group. *B*: weight of epididymal, inguinal, and retroperitoneal fat pads of wild-type and FS I-I Tg mice fed HFD from 4 to 13 wk of age. $*P < 0.05$, Student's *t*-test; $n = 5–6$ mice per group. *C*: weights of the tibialis anterior (TA), extensor digitorum longus (EDL), quadriceps femoris (QF), and soleus muscles from wild-type and FS I-I Tg mice fed a HFD from 4 to 13 wk of age. $*P < 0.005$, Student's *t*-test; $n = 5$ mice per group. *D*: triglycerides, NEFA, cholesterol, insulin, leptin, and adiponectin levels in wild-type and FS I-I Tg mice fed HFD from 4 to 13 wk of age. $*P < 0.0005$, $**P < 0.003$, $***P < 0.05$, $****P < 0.007$, Student's *t*-test; $n = 4–6$ mice per group. *E*: glucose tolerance test in wild-type and FS I-I Tg mice fed either normal diet (NFD) or HFD from 4 to 13 wk of age. Blood glucose was measured at 0, 15, 30, 60, and 120 min after glucose (dextrose) injection; $n = 6–8$ mice per group. $*P < 0.05$ and $**P < 0.01$, Student's *t*-test.

in FS I-I Tg and wild-type mice (Fig. 4*D*). Of note, triglyceride, NEFA, cholesterol, and leptin levels were lower in FS I-I Tg mice by 19.7, 13.6, 7.7, and 58.4%, respectively, compared with wild-type mice (Fig. 4*B* and Table 1). However, the serum adiponectin levels were 25.7% higher in FS I-I Tg mice than in wild-type mice when fed the HFD. By contrast, there were no significant differences in triglyceride, NEFA, cholesterol, leptin, and adiponectin levels between NFD-fed FS I-I Tg and wild-type mice (Table 1).

Defects in glucose homeostasis are important factors involved in the development of obesity. Therefore, we measured whole body glucose tolerance in FS I-I and wild-type mice fed the NFD or the HFD. Although there were no differences between NFD-fed FS I-I and wild-type mice, the glucose level tended to be lower in HFD-fed FS I-I Tg mice than in HFD-fed wild-type mice (Fig. 4*E*). These results indicate that the response to diet-induced obesity differs between FS I-I Tg and wild-type mice. In the NFD condition, no difference was observed in insulin tolerance (data not shown). However, in the HFD condition, FS I-I Tg mice exhibited better insulin tolerance than wild-type mice (Fig. S3).

FS I-I Tg mice are resistant to HFD-induced hepatic steatosis. As expected, the HFD increased hepatocyte lipid content and induced hepatic steatosis in wild-type mice. However, hepatic steatosis was not observed in HFD-fed FS I-I Tg mice (Fig. 5*A*). The liver from FS I-I Tg mice was histologically normal, even when these mice were fed the HFD, and showed significantly less lipid accumulation than HFD-fed

Table 1. *Serum metabolic parameters in wild-type and FS I-I Tg mice fed NFD or HFD*

	NFD		HFD	
Diet Treatment Genotype	Wild Type	FSI-I Tg	Wild Type	FSI-1 Tg
Triglyceride, mg/dl	108.5 ± 10.3	101.1 ± 7.5	122.8 ± 10.6	98.6 ± 7.5[a]
NEFA, mEq/l	0.83 ± 0.05	0.73 ± 0.09	0.97 ± 0.05	0.84 ± 0.04[b1]
Cholesterol, mg/dl	91.8 ± 4.9	81.2 ± 1.7	170.8 ± 7.7	157.6 ± 10.7[b2]
Fasting glucose, mg/dl	101.2 ± 16.2	107.8 ± 14.7	208.0 ± 2.0	208.0 ± 6.6
Insulin, ng/ml	0.91 ± 0.13	0.51 ± 0.12[b4]	2.16 ± 1.56	0.58 ± 0.34[c]
Leptin, ng/ml	4.00 ± 0.41	3.88 ± 0.14	21.35 ± 2.74	8.90 ± 3.88[d]
Adiponectin, μg/ml	21.0 ± 1.2	20.4 ± 1.3	35.1 ± 1.6	44.0 ± 2.4[b3]

Values are means ± SD; n = 4–6 mice per group. NFD, normal fat diet; HFD, high-fat diet; FSI I-I Tg, follistatin-derived peptide transgenic. a, b1–b3, c, and d, vs. wild-type mice (HFD); b4, vs. wild-type mice (NFD). [a]$P < 0.0005$; [b1–b4]$P < 0.003$; [c]$P < 0.05$; [d]$P < 0.007$ (Student's t-test).

wild-type mice (Fig. 5*A*). In addition, hepatic steatosis did not develop even in aged mice in FS I-I Tg mice (data not shown). The weight of the liver in HFD-fed FS I-I Tg mice was 13% less than that of wild-type mice (Fig. 5, *A* and *B*). The lower liver weight in FS I-I mice was attributed to reduced hepatocyte triglyceride accumulation in these mice compared with wild-type mice (Fig. 5*C*). Triglyceride contents in skeletal muscle were not significantly different between FS I-I mice and wild-type mice fed the HFD in our experimental condition (data not shown).

We next performed qPCR to determine the mRNA expression of genes related to fatty acid synthesis, including SCD1, which is required for the biosynthesis of monounsaturated fatty acids such as oleic acid and plays a key role in the hepatic synthesis of triglycerides (25). The hepatic SCD1 mRNA expression levels were 20% lower in HFD-fed FS I-I Tg mice than in wild-type mice (Fig. 6*A*). By contrast, the mRNA expression of ACC1 mRNA did not differ between FS I-I Tg and wild-type mice. We also measured the mRNA expression levels of Gck and PFK, two enzymes that regulate the glycolytic pathway. The expression levels of both genes were increased in FS I-I Tg mice compared with wild-type mice, 1.8-fold for GcK and 2-fold for PFK (Fig. 6*A*).

We measured hepatic fatty acid content in FS I-I Tg and wild-type mice. Interestingly, in HFD-fed mice, the fatty acid content and the ratio of fatty acids differed between the FS I-I Tg and wild-type mice. For example, the livers from HFD-fed FS I-I Tg mice showed an increased stearyl acid (C18:0) ratio and decreased oleic acid (C18:1) ratio to the total fatty acid content (Fig. 6*B* and Table 2). The absolute content of oleic acid (C18:1) and palmitoleic acid (C16:1) did not increase in FS I-I Tg mice compared with wild-type mice (Table 2). This finding is consistent with the decreased mRNA level of SCD1. Taken together, these results indicate that FS I-I Tg mice were resistant to hepatic steatosis induced by HFD and had reduced monounsaturated fatty acid content, particularly oleic acid (C18:1) and palmitoleic acid (C16:1).

DISCUSSION

Inhibition of myostatin is useful for various muscular diseases, including muscular dystrophies, muscular atrophy, cachexia induced by cancer, and sarcopenia (19, 34, 38). Furthermore, myostatin-null mice and myostatin propeptide-overexpressing Tg mice were used to study the effects of myostatin inhibition on obesity (10, 14, 24, 41, 42). These studies revealed that the inhibition of myostatin decreased adipose tissue accumulation and improved diet-induced obesity and genetic diabetes/obesity. The loss of myostatin in genetically obese mice partially suppressed adipose tissue accumulation and improved glucose metabolism (24). Meanwhile, upon high-fat feeding, the myostatin propeptide Tg mice showed favorable fat utilization and beneficial interactions between skeletal muscle and adipose tissues compared with control mice (42). Recent studies have suggested that inhibiting myostatin in muscle but not in adipose tissues is responsible for the decreased fat mass and improved insulin sensitivity (13). Indeed, inhibition of myostatin signaling in adipose tissue by ΔACVR2B had no effect on body composition, weight gain, or insulin tolerance either on NFD or on HFD. By contrast, inhibition of myostatin by ΔACVR2B in skeletal muscle resulted in increased lean mass, decreased fat mass, and improved glucose metabolism in mice fed an NFD or an HFD (13).

In our previous study, we reported the development and characterization of a novel myostatin inhibitor derived from follistatin, designated FS I-I. Although FS I-I showed significantly weaker inhibitory effects on activin, FS I-I retained its inhibitory effect on myostatin. In FS I-I Tg mice, inhibition of myostatin activity by FS I-I increased skeletal muscle mass and strength (27). Cardiac weight did not increase in FS I-I mice (Fig. S5). In this study, we have further demonstrated that Tg expression of the myostatin inhibitor FS I-I also has an antiobesity effect and improved glucose tolerance and prevents hepatic steatosis induced by HFD.

Various strategies can be exploited to inhibit myostatin, including neutralizing monoclonal myostatin antibodies, myostatin propeptide and ΔACVR2B (19). The neutralizing antibody is effective, but it can cause anti-idiotype immunity after in vivo administration. The myostatin propeptide is susceptible to proteolytic cleavage by members of the bone morphogenetic protein (BMP)-1/tolloid family of metalloproteinases, impairing its ability to inhibit myostatin (40). Purified follistatin has several cleaved isoforms; the COOH-terminal region is susceptible to proteinase cleavage, although the cleaved follistatin molecules can still inhibit activin and myostatin (36). FS I-I comprises the NH_2-terminal region and two consecutive follistatin domain I regions. Therefore, FS I-I lacks the native follistatin COOH-terminal region, which is susceptible to protease cleavage. Furthermore, follistatin is a naturally occurring peptide and may cause fewer immune responses than exogenous antibodies. Therefore, among myostatin inhibitors, FS I-I offers some advantages over monoclonal antibodies and myostatin propeptide.

Adipocytes in FS I-I Tg mice contained fewer lipids than wild-type mice when they were fed a standard diet. Therefore,

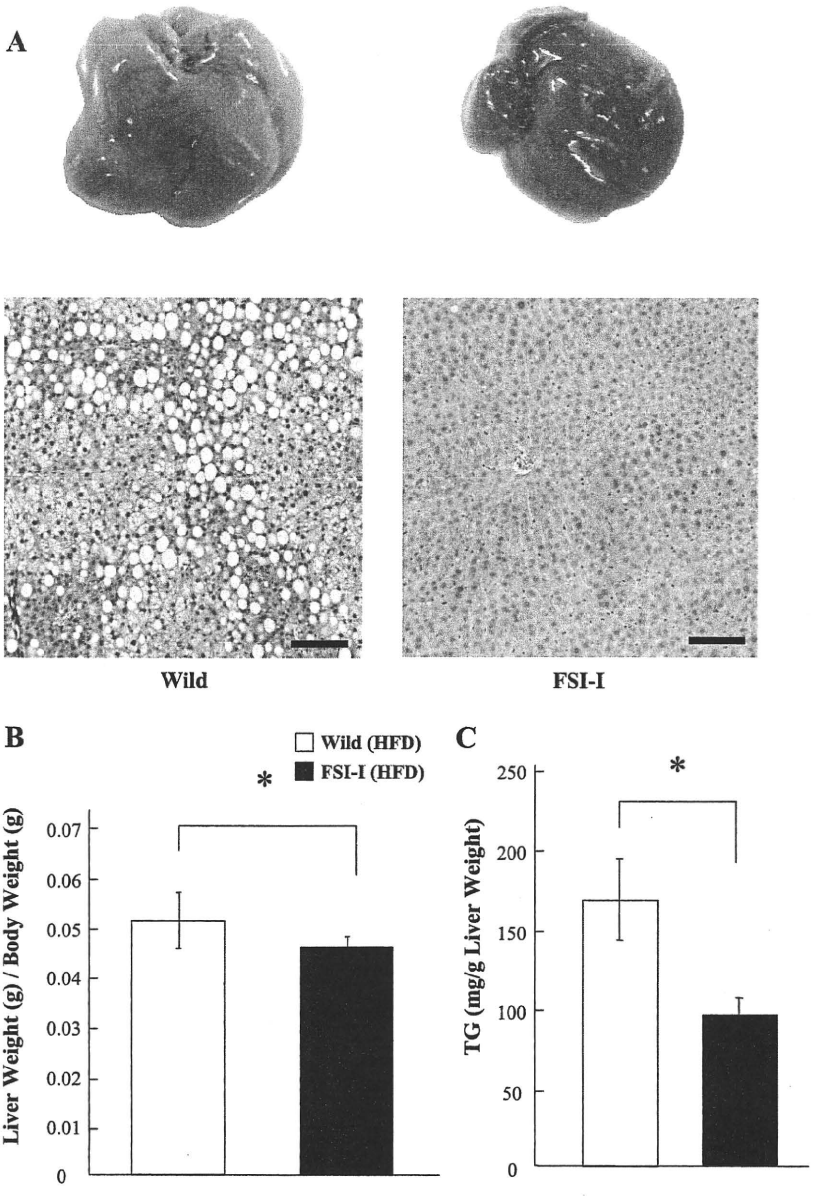

Fig. 5. *A*: morphology of liver samples from 13-wk-old wild-type and FS I-I Tg fed HFD. Liver sections were analyzed with H&E staining (*bottom*). Scale bar, 100 μm. *B*: relative liver weight (g) to body weight (g) of wild-type and FS I-I Tg mice fed HFD from 4 to 13 wk of age; $n = 6$ mice per group. $^*P < 0.01$, Student's *t*-test. *C*: hepatic triglyceride (TG) content in wild-type and FS I-I Tg mice fed HFD from 4 to 13 wk of age; $n = 5$ mice per group. $^*P < 0.0005$, Student's *t*-test.

mean adipocyte size was smaller in FS I-I Tg mice than in wild-type mice (Fig. 1, *B–D*). By contrast, fat mass was normal in myostatin propeptide Tg mice fed a standard diet (42). During HFD feeding, myostatin knockout mice gained fat mass, whereas muscle weight was unaffected by the HFD. By contrast, in FS I-I Tg mice, the skeletal muscle mass was still increased, albeit blunted compared with control mice (27, 42). The differences in the increases of fat and skeletal muscle mass in these models might be due to how much endogenous active myostatin is present in vivo.

We examined the expression levels of mRNAs encoding UCPs. The adipose tissue in FS I-I Tg mice showed upregulation of UCP3 mRNA expression levels (Fig. 2*A*) but not UCP1 or UCP2 compared with wild-type mice (data not shown). While UCP2 shows rather ubiquitous expression, UCP1 is specifically expressed in brown adipocytes and UCP3 is specifically expressed in skeletal muscle, brown adipose tissues, and heart (6, 18). Upregulation of UCP3 mRNA expression levels in FS I-I Tg mice was thought to increase energy expenditure. In addition, we observed adipose tissue by transmission electron microscopy (Fig. 2*C*). We found that the adipocytes in FS I-I Tg mice contained increased numbers of mitochondria. The mitochondria in FS I-I Tg adipocyte contained mitochondrial cristae, suggesting that they had normal mitochondrial function. To our knowledge, this is the first report demonstrating that myostatin inhibition causes an apparent increase in mitochondria abundance. The biogenesis of mitochondria requires coordinated protein synthesis and as-

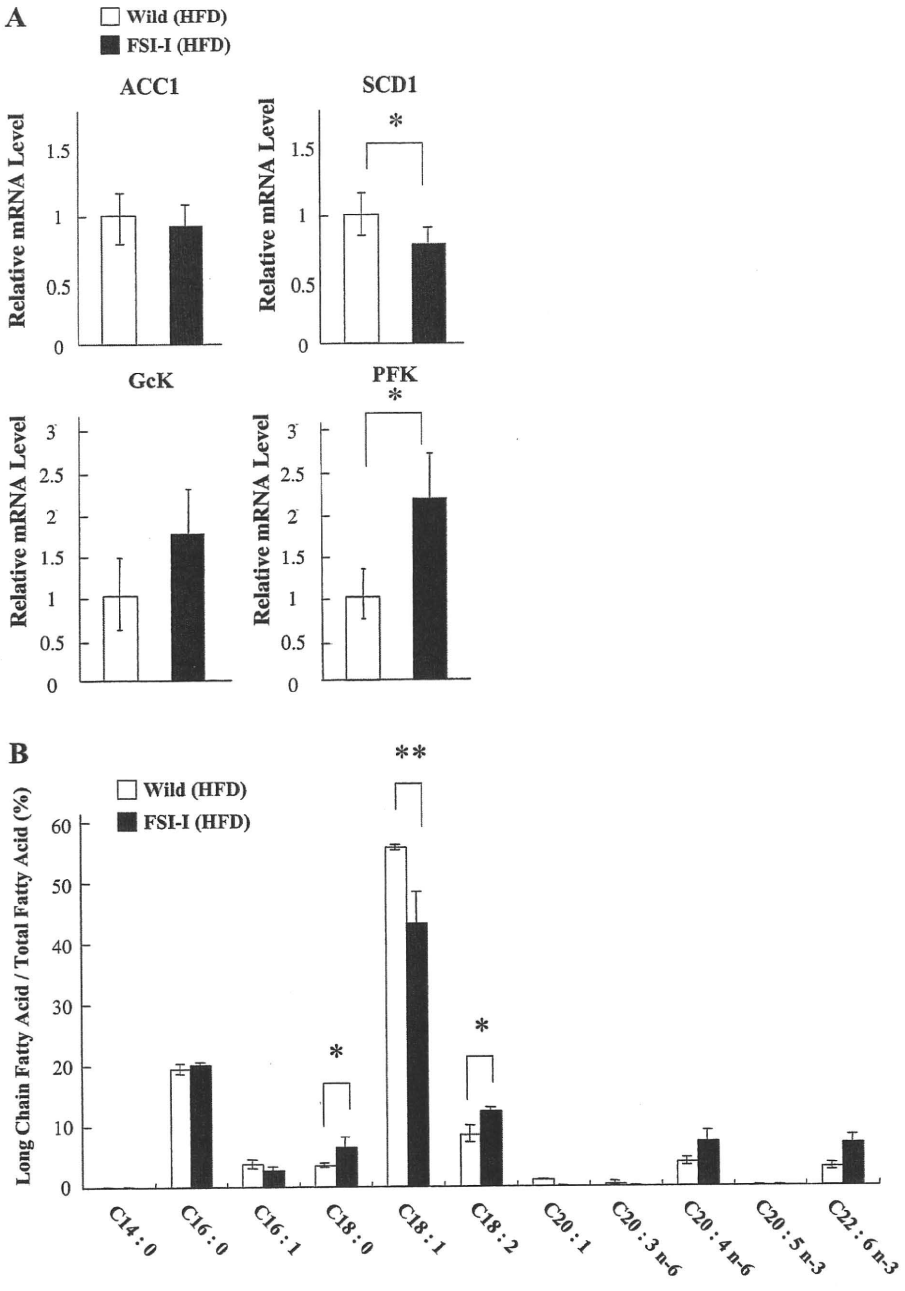

Fig. 6. *A*: relative hepatic mRNA expression levels of ACC1, SCD1, Gck, and PFK were measured by qPCR in wild-type and FS I-I Tg mice fed HFD; $n = 5$ mice per group. $^*P < 0.05$, Student's *t*-test. *B*: ratio of long-chain fatty acids to total fatty acids in liver of wild-type and FS I-I Tg mice fed HFD; $n = 6$ mice per group. $^*P < 0.05$ and $^{**}P < 0.03$, Student's *t*-test.

sembly from both the nuclear and mitochondrial genomes. Mitochondrial abundance can be modulated in response to physical activity, metabolic demands, and nutrition (16). PPARγ ligands increase mitochondrial biogenesis in white adipose tissue, and the PPARγ coactivator-1 (PGC-1) family is well characterized as a pivotal transcriptional coactivator for mitochondrial biogenesis (16). Although the mechanism of how mitochondria number and size are increased in adipocytes of FS I-I Tg mice remains to be determined, one possible mechanism may be upregulation of the PGC-1-dependent transcription cascade in white adipose tissues. Alternatively, it is also possible that the rate of mitochondrial turnover could be changed in white adipocytes of FS I-I Tg mice. Energy expenditure in FS I-I Tg mice was influenced by increased muscle mass, whereas adipose tissue is involved in energy storage. Therefore, changes in mitochondria abundance in adipocytes could modulate whole body energy expenditure and storage.

The insulin level in HFD-fed FS I-I Tg mice was lower than that in control mice (Fig. 4*D*), but glucose tolerance was better in HFD-fed FS I-I Tg mice than in HFD-fed wild-type mice. FS I-I is expressed under a skeletal muscle-specific myosin light-chain promoter and shows a widespread increase in muscle mass. The expression of FSI-I is restricted to skeletal muscles and is not detected in adipose tissues, liver, or serum (Fig. 3*A*). The circulating level of FSI-I in serum is under the detection limit and low compared with that of follistatin.

Table 2. *Hepatic fatty acid in wild-type and FS I-I Tg mice fed NFD or HFD*

Diet Treatment	NFD		HFD	
Genotype	Wild Type	FSI-I Tg	Wild Type	FSI-I Tg
C14:0	ND	ND	ND	ND
C16:0	13.1 ± 7.2	10.5 ± 4.9	20.2 ± 4.9	10.5 ± 2.8[a1]
C16:1	2.1 ± 1.7	1.3 ± 0.9	3.8 ± 1.1	1.5 ± 0.6[a2]
C18:0	3.0 ± 0.4	3.3 ± 1.0	3.5 ± 0.4	3.2 ± 0.1
C18:1	27.1 ± 22.1	21.4 ± 17.3	57.8 ± 12.0	23.1 ± 9.4[b]
C18:2	7.2 ± 2.1	6.7 ± 2.0	8.9 ± 2.7	6.4 ± 1.5
C20:1	0.3 ± 0.5	ND	1.1 ± 0.2	ND
C20:3n-6	0.1 ± 0.2	0.1 ± 0.2	0.4 ± 0.3	ND
C20:4n-6	3.0 ± 1.0	3.4 ± 1.5	3.9 ± 0.2	3.6 ± 0.1
C22:6n-3	3.4 ± 0.9	3.6 ± 1.0	3.1 ± 0.7	3.5 ± 0.3
Total	59.3 ± 35.9	50.3 ± 28.1	102.7 ± 22	51.8 ± 14.9

Values are means ± SD; $n = 6$ mice per group. ND, not detected (μg/mg). a1–a2 and b, vs. wild-type mice (HFD); $^{a1-a2}P < 0.05$; $^{b}P < 0.02$ (Student's *t*-test).

Furthermore, a 30.2% reduction of phosphorylated Smad 3, representing lower myostatin signaling, was detected in skeletal muscles but not in other tissues (Fig. 3*B*). Therefore, it is likely that myostatin signaling in muscle, rather than the direct effects of myostatin on adipose tissue, is responsible for the decrease in fat mass in FS I-I Tg mice. We also studied the effects of myostatin and FS I-I in Hep G2 cells and 3T3-L1 cell lines. In both cases, the triglyceride level was not affected either by myostatin or by follistatin-derived peptide stimulation (Fig. S4), supporting the secondary and indirect effects of FS I-I on adipocytes and hepatocytes. The increased skeletal muscle mass may have greater capacity for glucose uptake, reducing substrate supply for hepatic lipogenesis.

The normal age-dependent adipose tissue accumulation was decreased in NFD-fed FS I-I Tg mice (Fig. 1*A*). Intriguingly, the adipocytes were smaller as a result of myostatin inhibition by FS I-I (Fig. 1, *B–D*), reflecting reduced lipid accumulation. Obesity occurs when the adipose tissue is overloaded with high-energy nutrients and energy expenditure is reduced. Therefore, we studied the effect of diet-induced obesity in FS I-I Tg and wild-type mice. The body weight of HFD-fed FS I-I Tg mice was comparable with that of HFD-fed wild-type mice (Fig. 4*A*), which was attributed to the increase in muscle weight and decrease in adipose tissue and liver weights in FS I-I Tg mice (Fig. 4, *B* and *C*). Interestingly, there is a report that mice with an insertion allele at the *Inhba* locus, $Inhba^{BK}$, are smaller and leaner than wild-type littermate (20). In $Inhba^{BK}$ mice, the sequences of the mature activin-βA domain were replaced with the corresponding sequences from activin-βB. $Inhba^{BK}$ mice have less adipose tissue than wild-type littermates. The growth of $Inhba^{BK}$ is improved by providing an HFD to a level comparable with that of wild-type mice on an NFD (20). The phenotype of FS I-I mice with lower myostatin signaling is different from that of $Inhba^{BK}$ mice. Therefore, although activin A and myostatin are functionally similar to maintain energy balance and regulate skeletal muscle mass, they may have different functions in vivo. As would be expected, the HFD increased the levels of cholesterol, fasting glucose, insulin, and leptin (Fig. 4*D* and Table 1) compared with the NFD in wild-type mice (Table 1). However, the triglyceride, NEFA, cholesterol, insulin, and leptin levels were lower in HFD-fed FS I-I Tg mice than in HFD-fed wild-type mice (Table 1 and Fig. 4*D*). Furthermore, we observed an increase in serum adiponectin in FS I-I Tg mice (Table 1). These results are similar to those of myostatin-null mice and myostatin propeptide Tg mice (13, 42). Interestingly, the HFD-fed FS I-I Tg mice exhibited better glucose tolerance than HFD-fed wild type mice (Fig. 4*E*). By contrast, in mice fed the NFD, glucose tolerance was similar in FS I-I Tg and wild-type mice. This differs from the situation in myostatin knockout mice, because myostatin knockout mice showed improved glucose tolerance, even when they were fed the NFD (24). With respect to whole body metabolism, we performed indirect calorimetric analyses. Although food intake was not significantly different between wild-type and FS I-I mice, the metabolic rate calculated from $\dot{V}o_2$ was increased in FS I-I Tg compared with control. When normalized with body weight, no statistically significant difference was observed (Supplementary Table S1). Collectively, these results indicate that FS I-I Tg mice were resistant to HFD-induced obesity and showed improved glucose tolerance during excess energy intake.

Intriguingly, FS I-I Tg mice were resistant to hepatic steatosis during high-fat feeding, which was confirmed by histology, liver weight, and liver fatty acid accumulation (Fig. 5, *A–C* and Table 2). The hepatic histology of HFD-fed FS I-I Tg mice did not show any difference to NFD-fed wild-type mice. The hepatic expression level of SCD1 mRNA was lower in FS I-I Tg mice than in wild-type mice. SCD1 is a rate-limiting lipogenic enzyme required for the synthesis of monounsaturated fatty acids and plays a key role in the hepatic synthesis of triglycerides. As a result of decreased SCD1 expression, the hepatic content of oleic acid (C18:1) and palmitoleic acid (C16:1), monounsaturated fatty acids produced by SCD1, was decreased (Fig. 6*B* and Table 2). A decrease in SCD1 expression was reported to be responsible for the prevention of diet-induced obesity, insulin resistance, and diabetes (9, 28). Furthermore, SCD1-null mice were resistant to diet-induced obesity and hepatic steatosis (9). The resistance of FS I-I Tg mice to HFD-induced obesity and hepatic steatosis may, in part, involve the reduced mRNA expression of SCD1. Changes of RNA and protein end points represent lower adiposity and lower hepatic fat levels. The lower adiposity is likely secondary to increased muscle mass and lower myostatin signaling in skeletal muscle.

The increase in skeletal muscle mass and reduction in fat mass would likely take at least several months to occur. Meanwhile, injection of myostatin neutralizing antibody does not decrease the adipose tissue mass (35, 39). However, even if the fat mass is not decreased, it seems likely that the inhibition of myostatin improves glucose tolerance and insulin sensitivity and prevents hepatic steatosis due to lower insulin levels, increased adiponectin levels, and changes in substrate utilization in skeletal muscle, adipose tissue, and liver. In summary, the inhibition of myostatin by various strategies, including follistatin-derived peptide, may offer a novel therapy against obesity, diabetes, and hepatic steatosis.

ACKNOWLEDGMENTS

We thank Drs. K. Hitachi, A. Uezumi, and H. Ageta for discussion and advice. We also thank S. Sato and A. Yamaguchi for technical assistance.

GRANTS

This research was partly supported by a Grant-in-Aid for Scientific Research (21590320 to K. Tsuchida) from the Japan Society for the Promotion of Science, a Grant-in-Aid for Young Scientists (22790328 to M. Nakatani) from JSPS, a research grant (H20-018) on psychiatric and neurological diseases and mental health from the Ministry of Health, Labour and Welfare, and an Intramural Research Grant (20B-13) for Neurological and Psychiatric Disorders of National Center of Neurology and Psychiatry.

DISCLOSURES

No conflicts of interest are reported by the authors.

REFERENCES

1. **Akpan I, Goncalves MD, Dhir R, Yin X, Pistilli EE, Bogdanovich S, Khurana TS, Ucran J, Lachey J, Ahima RS.** The effects of a soluble activin type IIB receptor on obesity and insulin sensitivity. *Int J Obes (Lond)* 33: 1265–1273, 2009.
2. **Amthor H, Nicholas G, McKinnell I, Kemp CF, Sharma M, Kambadur R, Patel K.** Follistatin complexes Myostatin and antagonises Myostatin-mediated inhibition of myogenesis. *Dev Biol* 270: 19–30, 2004.
3. **Archibald FM, Skipski VP.** Determination of fatty acid content and composition in ultramicro lipid samples by gas-liquid chromatography. *J Lipid Res* 7: 442–445, 1966.
4. **Bligh EG, Dyer WJ.** A rapid method of total lipid extraction and purification. *Can J Biochem Physiol* 37: 911–917, 1959.
5. **Boman IA, Klemetsdal G, Blichfeldt T, Nafstad O, Vage DI.** A frameshift mutation in the coding region of the myostatin gene (MSTN) affects carcass conformation and fatness in Norwegian White Sheep (*Ovis aries*). *Anim Genet* 40: 418–422, 2009.
6. **Brand MD, Esteves TC.** Physiological functions of the mitochondrial uncoupling proteins UCP2 and UCP3. *Cell Metab* 2: 85–93, 2005.
7. **Chan CB, Harper ME.** Uncoupling proteins: role in insulin resistance and insulin insufficiency. *Curr Diabetes Rev* 2: 271–283, 2006.
8. **Clop A, Marcq F, Takeda H, Pirottin D, Tordoir X, Bibe B, Bouix J, Caiment F, Elsen JM, Eychenne F, Larzul C, Laville E, Meish F, Milenkovic D, Tobin J, Charlier C, Georges M.** A mutation creating a potential illegitimate microRNA target site in the myostatin gene affects muscularity in sheep. *Nat Genet* 38: 813–818, 2006.
9. **Dobrzyn A, Ntambi JM.** Stearoyl-CoA desaturase as a new drug target for obesity treatment. *Obes Rev* 6: 169–174, 2005.
10. **Feldman BJ, Streeper RS, Farese RV Jr, Yamamoto KR.** Myostatin modulates adipogenesis to generate adipocytes with favorable metabolic effects. *Proc Natl Acad Sci USA* 103: 15675–15680, 2006.
11. **Gamer LW, Cox KA, Small C, Rosen V.** Gdf11 is a negative regulator of chondrogenesis and myogenesis in the developing chick limb. *Dev Biol* 229: 407–420, 2001.
12. **Gilson HM, Schakman OR, Kalista S, Lause P, Tsuchida K, Thissen JP.** Follistatin induces muscle hypertrophy through satellite cell proliferation and inhibition of both myostatin and activin. *Am J Physiol Endocrinol Metab* 297: E157–E164, 2009.
13. **Guo T, Jou W, Chanturiya T, Portas J, Gavrilova O, McPherron AC.** Myostatin inhibition in muscle, but not adipose tissue, decreases fat mass and improves insulin sensitivity. *PLoS One* 4: e4937, 2009.
14. **Hamrick MW, Pennington C, Webb CN, Isales CM.** Resistance to body fat gain in "double-muscled" mice fed a high-fat diet. *Int J Obes (Lond)* 30: 868–870, 2006.
15. **Hill JJ, Davies MV, Pearson AA, Wang JH, Hewick RM, Wolfman NM, Qiu Y.** The myostatin propeptide and the follistatin-related gene are inhibitory binding proteins of myostatin in normal serum. *J Biol Chem* 277: 40735–40741, 2002.
16. **Hock MB, Kralli A.** Transcriptional control of mitochondrial biogenesis and function. *Annu Rev Physiol* 71: 177–203, 2009.
17. **Ishigaki Y, Katagiri H, Yamada T, Ogihara T, Imai J, Uno K, Hasegawa Y, Gao J, Ishihara H, Shimosegawa T, Sakoda H, Asano T, Oka Y.** Dissipating excess energy stored in the liver is a potential treatment strategy for diabetes associated with obesity. *Diabetes* 54: 322–332, 2005.
18. **Krauss S, Zhang CY, Lowell BB.** The mitochondrial uncoupling-protein homologues. *Nat Rev Mol Cell Biol* 6: 248–261, 2005.
19. **Lee SJ.** Regulation of muscle mass by myostatin. *Annu Rev Cell Dev Biol* 20: 61–86, 2004.
20. **Li L, Shen JJ, Bournat JC, Huang L, Chattopadhyay A, Li Z, Shaw C, Graham BH, Brown CW.** Activin signaling: effects on body composition and mitochondrial energy metabolism. *Endocrinology* 150: 3521–3529, 2010.
21. **McPherron AC, Huynh TV, Lee SJ.** Redundancy of myostatin and growth/differentiation factor 11 function. *BMC Dev Biol* 9: 24, 2009.
22. **McPherron AC, Lawler AM, Lee SJ.** Regulation of skeletal muscle mass in mice by a new TGF-beta superfamily member. *Nature* 387: 83–90, 1997.
23. **McPherron AC, Lee SJ.** Double muscling in cattle due to mutations in the myostatin gene. *Proc Natl Acad Sci USA* 94: 12457–12461, 1997.
24. **McPherron AC, Lee SJ.** Suppression of body fat accumulation in myostatin-deficient mice. *J Clin Invest* 109: 595–601, 2002.
25. **Miyazaki M, Flowers MT, Sampath H, Chu K, Otzelberger C, Liu X, Ntambi JM.** Hepatic stearoyl-CoA desaturase-1 deficiency protects mice from carbohydrate-induced adiposity and hepatic steatosis. *Cell Metab* 6: 484–496, 2007.
26. **Mosher DS, Quignon P, Bustamante CD, Sutter NB, Mellersh CS, Parker HG, Ostrander EA.** A mutation in the myostatin gene increases muscle mass and enhances racing performance in heterozygote dogs. *PLoS Genet* 3: e79, 2007.
27. **Nakatani M, Takehara Y, Sugino H, Matsumoto M, Hashimoto O, Hasegawa Y, Murakami T, Uezumi A, Takeda S, Noji S, Sunada Y, Tsuchida K.** Transgenic expression of a myostatin inhibitor derived from follistatin increases skeletal muscle mass and ameliorates dystrophic pathology in mdx mice. *FASEB J* 22: 477–487, 2008.
28. **Ntambi JM, Miyazaki M.** Recent insights into stearoyl-CoA desaturase-1. *Curr Opin Lipidol* 14: 255–261, 2003.
29. **Ohsawa Y, Hagiwara H, Nakatani M, Yasue A, Moriyama K, Murakami T, Tsuchida Noji S K, Sunada Y.** Muscular atrophy of caveolin-3-deficient mice is rescued by myostatin inhibition. *J Clin Invest* 116 : 2924–2934, 2006.
30. **Pangas SA, Jorgez CJ, Tran M, Agno J, Li X, Brown CW, Kumar TR, Matzuk MM.** Intraovarian activins are required for female fertility. *Mol Endocrinol* 21: 2458–2471, 2007.
31. **Saito S, Sugino K, Yamanouchi K, Kogawa K, Titani K, Shiota K, Takahashi M, Sugino H.** Characterization of antisera directed against follistatin/activin-binding protein peptides. *Endocrinol Jpn* 38: 377–382, 1991.
32. **Schuelke M, Wagner KR, Stolz LE, Hubner C, Riebel T, Komen W, Braun T, Tobin JF, Lee SJ.** Myostatin mutation associated with gross muscle hypertrophy in a child. *N Engl J Med* 350: 2682–2688, 2004.
33. **Shelton GD, Engvall E.** Gross muscle hypertrophy in whippet dogs is caused by a mutation in the myostatin gene. *Neuromuscul Disord* 17: 721–722, 2007.
34. **Siriett V, Salerno MS, Berry C, Nicholas G, Bower R, Kambadur R, Sharma M.** Antagonism of myostatin enhances muscle regeneration during sarcopenia. *Mol Ther* 15: 1463–1470, 2007.
35. **Stolz LE, Li D, Qadri A, Jalenak M, Klaman LD, Tobin JF.** Administration of myostatin does not alter fat mass in adult mice. *Diabetes Obes Metab* 10: 135–142, 2008.
36. **Sugino K, Kurosawa N, Nakamura T, Takio K, Shimasaki S, Ling N, Titani K, Sugino H.** Molecular heterogeneity of follistatin, an activin-binding protein. Higher affinity of the carboxyl-terminal truncated forms for heparan sulfate proteoglycans on the ovarian granulosa cell. *J Biol Chem* 268: 15579–15587, 1993.
37. **Tsuchida K.** Activins, myostatin and related TGF-beta family members as novel therapeutic targets for endocrine, metabolic and immune disorders. *Curr Drug Targets Immune Endocr Metabol Disord* 4: 157–166, 2004.
38. **Tsuchida K.** Targeting myostatin for therapies against muscle-wasting disorders. *Curr Opin Drug Discov Devel* 11: 487–494, 2008.
39. **Whittemore LA, Song K, Li X, Aghajanian J, Davies M, Girgenrath S, Hill JJ, Jalenak M, Kelley P, Knight A, Maylor R, O'Hara D, Pearson A, Quazi A, Ryerson S, Tan XY, Tomkinson KN, Veldman GM, Widom A, Wright JF, Wudyka S, Zhao L, Wolfman NM.** Inhibition of myostatin in adult mice increases skeletal muscle mass and strength. *Biochem Biophys Res Commun* 300: 965–971, 2003.
40. **Wolfman NM, McPherron AC, Pappano WN, Davies MV, Song K, Tomkinson KN, Wright JF, Zhao L, Sebald SM, Greenspan DS, Lee SJ.** Activation of latent myostatin by the BMP-1/tolloid family of metalloproteinases. *Proc Natl Acad Sci USA* 100: 15842–15846, 2003.
41. **Yang J, Zhao B.** Postnatal expression of myostatin propeptide cDNA maintained high muscle growth and normal adipose tissue mass in transgenic mice fed a high-fat diet. *Mol Reprod Dev* 73: 462–469, 2006.
42. **Zhao B, Wall RJ, Yang J.** Transgenic expression of myostatin propeptide prevents diet-induced obesity and insulin resistance. *Biochem Biophys Res Commun* 337: 248–255, 2005.

Development, Growth & Differentiation
The Japanese Society of Developmental Biologists

Develop. Growth Differ. (2011) **53**, 48–54 doi: 10.1111/j.1440-169X.2010.01221.x

Original Article

Atelocollagen-mediated systemic administration of myostatin-targeting siRNA improves muscular atrophy in caveolin-3-deficient mice

Emi Kawakami,[1†] Nao Kinouchi,[1†] Taro Adachi,[2] Yutaka Ohsawa,[3] Naozumi Ishimaru,[4] Hideyo Ohuchi,[2] Yoshihide Sunada,[3] Yoshio Hayashi,[4] Eiji Tanaka[1] and Sumihare Noji[2*]

[1]*Department of Orthodontics and Dentofacial Orthopedics, Institute of Health Bioscience, The University of Tokushima Graduate School, 3-18-15 Kuramoto, Tokushima 770-8504;* [2]*Department of Life Systems, Institute of Technology and Science, The University of Tokushima, 2-1 Minami-Jyosanjima-cho, Tokushima 770-8506;* [3]*Department of Neurology, Kawasaki Medical School, 577 Matsushima, Kurashiki City, Okayama 701-0192; and* [4]*Department of Oral Molecular Pathology, Institute of Health Bioscience, The University of Tokushima Graduate School, 3-18-15 Kuramoto, Tokushima 770-8504, Japan*

Small interfering RNA (siRNA)-mediated silencing of gene expression is rapidly becoming a powerful tool for molecular therapy. However, the rapid degradation of siRNAs and their limited duration of activity require efficient delivery methods. Atelocollagen (ATCOL)-mediated administration of siRNAs is a promising approach to disease treatment, including muscular atrophy. Herein, we report that ATCOL-mediated systemic administration of a myostatin-targeting siRNA into a caveolin-3-deficient mouse model of limb-girdle muscular dystrophy 1C (LGMD1C) induced a marked increase in muscle mass and a significant recovery of contractile force. These results provide evidence that ATCOL-mediated systemic administration of siRNAs may be a powerful therapeutic tool for disease treatment, including muscular atrophy.

Key words: atelocollagen, muscle, muscular dystrophy, myostatin, RNA interference.

Introduction

Myostatin (growth differentiation factor 8, GDF8) is a member of the transforming growth factor-β (TGF-β) superfamily of secreted growth factors (McPherron *et al.* 1997). A number of growth factors of this family have been shown to regulate cell growth and differentiation during development. Myostatin is unique among the members of the TGF-β superfamily because its expression is almost exclusively restricted to the skeletal muscle lineage.

Zhu *et al.* (2000) generated transgenic mice that expressed myostatin mutated at its cleavage site under the control of a muscle specific promoter creating a dominant negative myostatin. These mice exhibited a significant (20–35%) increase in muscle mass that resulted from myofiber hypertrophy and not from myofiber hyperplasia. While, mice fully null for myostatin showed muscle masses that were nearly double that of normal muscle and this marked increase in muscle mass was associated with both hypertrophy and hyperplasia (McPherron *et al.* 1997). The difference in muscle mass seen in dominant negative myostatin and null myostatin mice likely results from incomplete dominance of dominant negative myostatin, so that dimerization and cleavage of normal myostatin is not fully blocked in dominant negative myostatin mice. So, lower levels of myostatin inhibition may affect hypertrophy, while higher levels of myostatin inhibition may be required to alter hyperplasia (Zhu *et al.* 2000). Thus, it appears that myostatin specifically downregulates skeletal muscle mass.

Because of its inhibitory role, myostatin downregulation may serve as a potentially important mechanism for treating diseases associated with muscle wasting and degeneration, such as muscular dystrophy. We recently demonstrated that myostatin inhibition induced by overexpression of the myostatin pro-domain prevented

*Author to whom all correspondence should be addressed.
Email: noji@bio.tokushima-u.ac.jp
†These authors contributed equally to this work.
Received 6 August 2010; revised 4 October 2010; accepted 4 October 2010.

muscular atrophy and normalized intracellular myostatin signaling in a mouse model of limb-girdle muscular dystrophy 1C (LGMD1C) (Nishi *et al.* 2002). Furthermore, myostatin inhibition also suppressed muscular atrophy in caveolin-3-deficient mice that expressed a dominant-negative form of the caveolin-3 gene (Ohsawa *et al.* 2006). The dominant negative caveolin-3 mutation was a missense mutation (Pro104Leu) that was expressed under the control of the M-creatine kinase promoter (Sunada *et al.* 2001).

Duchenne muscular dystrophy (DMD) is an X-linked, lethal skeletal muscle disorder caused by mutations in the *dystrophin* gene (Bulfield *et al.* 1984; Yoshimura *et al.* 2007); it is a severe muscle wasting disorder that affects 1/3500 male births (Deconinck & Dan 2007). To date, there is no effective treatment for muscular dystrophy, although gene therapy could be a valuable approach to treating this disease. In a previous study, inhibition of myostatin using anti-myostatin blocking antibodies was employed in an effort to increase muscle mass (Bogdanovich *et al.* 2002). However, the generation of antibodies against recombinant target proteins was a time-consuming, labor-intensive approach.

Recently, RNA interference (RNAi) has emerged as an effective gene silencing method. RNAi refers to sequence-specific, post-transcriptional gene silencing mediated by approximately 22-nucleotide-long small interfering RNAs (siRNAs) generated from longer double-stranded RNAs (dsRNAs) in both plants and animals, ranging from flatworms to humans (Fire *et al.* 1998). RNAi-based approaches have increasingly been developed in which highly specific siRNAs designed to target disease-causing or disease-promoting genes are utilized without the induction of interferon synthesis or non-specific gene suppression (Elbashir *et al.* 2001; de Fougerolles *et al.* 2007). Magee *et al.* (2006) demonstrated that downregulation of myostatin expression via electroporation of a plasmid directing the expression of a short hairpin interfering RNA (shRNA) against myostatin led to a localized increase in skeletal muscle mass. For safety reasons, however, strategies using vector-based delivery systems may be of limited clinical use. Therefore, a more desirable approach would involve the direct application of active siRNAs *in vivo*.

Atelocollagen (ATCOL), a pepsin-treated type I collagen that lacks antigenicity-conferring telopeptides at its N and C termini, has been shown to promote the efficient delivery of chemically unmodified siRNAs to metastatic tumors *in vivo* (Minakuchi *et al.* 2004; Takeshita *et al.* 2005; Takeshita & Ochiya 2006). Based on its practical use as an siRNA delivery platform, we adapted an ATCOL-mediated oligonucleotide system to deliver a myostatin-targeting siRNA into muscle, and found that local or systemic administration of the myostatin-targeting siRNA coupled with ATCOL led to a marked stimulation of muscle growth *in vivo* within a few weeks (Kinouchi *et al.* 2008). In the current study, we examined whether systemic administration of the myostatin-siRNA/ATCOL (Mst-siRNA/ATCOL) complex effectively silenced myostatin expression in LGMD1C mice, and whether it led to increased muscle mass and/or decreased muscle weakness. In the current study, we used the same myostatin-targeting siRNA reported previously (Magee *et al.* 2006), which is predicted to target myostatin mRNA not only in mice, but also in humans, rats, cows, macaques, and baboons.

Materials and methods

Systemic administration of the Mst-siRNA/ATCOL complex to skeletal muscles in LGMD1C mice

The Mst-siRNA and ATCOL complexes were prepared as follows. Equal volumes of siRNA solution (siRNA and 1× siRNA buffer, 40 μmol/L final concentration) and ATCOL (0.05% final concentration) were combined and mixed by vigorous pipetting. For systemic administration, the siRNA/ATCOL complex (200 μL) was introduced intravenously via orbital veins into 20-week-old LGMD1C mice at 0, 4, 7 and 14 days. As a negative control, scrambled siRNAs were injected into 20-week-old LGMD1C mice at 0, 4, 7 and 14 days.

Morphometric analyses

The masseter and quadriceps femoris muscle tissues were dissected 3 weeks after the first Mst-siRNA/ATCOL complex administration. The tissues were snap-frozen in liquid nitrogen-cooled isopentane and sectioned transversely (6 μm) at the center of the masseter and quadriceps femoris muscles using a cryostat (Leica Microsystems). Sections were stained with hematoxylin and eosin (H&E), and fiber sizes were determined by measuring the area of each transversal myofiber within a fixed area. Approximately 100 myofibers were measured for each tissue sample (six to eight fields/tissue section).

Contractile properties of Mst-siRNA/ATCOL complex-treated tibials anterior (TA) muscles

The entire tibials anterior (TA) muscle was removed with its tibial origin intact, and the distal portion of the TA tendon, together with its origin, were secured with a 5-0 silk suture. The TA was then mounted in a vertical tissue chamber and connected to a force transducer, UL-10GR (Minerva, Nagano, Japan), and a length servosystem, MM-3 (Narishige, Tokyo, Japan).

Electrical stimulations were applied using a SEN3301 (Nihon Kohden, Tokyo, Japan) through a pair of platinum wires placed on both sides of the muscle in physiological salt solution (150 mmol/L NaCl, 4 mmol/L KCl, 2 mmol/L $CaCl_2$, 1 mmol/L $MgCl_2$, 5.6 mmol/L glucose, 5 mmol/L Hepes, pH 7.4, and 0.02 mmol/L D-tubocurarine). Muscle fiber length was adjusted incrementally using a micropositioner until peak isometric twitch force responses were obtained (optimal fiber length [L_O]). Maximal tetanic force (P_O) was assessed by stimulation frequencies of 125 pulses/s delivered in 500 ms duration trains with 2 min intervals between each train. After two measurements were taken, the stimulated muscles were weighted after the tendon and bone attachments were removed. All forces were normalized to the physiological cross-sectional area (pCSA), the latter estimated on the basis of the following formula: muscle wet weight (in mg)/(L_O [in mm] x 1.06 [in mg/mm^3]). The estimated pCSA was used to determine specific tetanic force, and the muscle was quickly frozen in liquid nitrogen-cooled isopentane for morphometric analysis.

Statistical analyses

Error bars indicate standard deviation of the mean. * indicates $P < 0.01$ or $P < 0.05$ in a Student's *t* test.

Results

The Mst-siRNA/ATCOL complex can stabilize and produce a long-term gene silencing effect

In initial experiments to evaluate the persistence and spread of siRNA/ATCOL complexes (100 μL), we injected a BLOCK-iT Alexa Fluor Red Fluorescent Oligo (10 μmol/L) in the masseter muscle of 20-week-old C57BL/6 mice. Mice were killed at 2 weeks, tissue samples were dissected, and Alexa Fluor Red Fluorescent Oligo expression was assessed under conditions identical to those used in myostatin gene transfer experiments. As expected, Alexa Fluor Red Fluorescent Oligo expression was detected near the sites of injection with an uneven distribution pattern across the tissue (Fig. 1, right panel). These observations suggested that the ATCOL and siRNA formed a stable complex capable of producing an efficient, long-term gene silencing effect.

Intravenous administration of myostatin-targeting siRNAs with ATCOL specifically repressed muscle atrophy in LGMD1C mice

Based on our observation that ATCOL formed stable complexes with siRNAs capable of long-term gene silencing, we administered Mst-siRNA/ATCOL or control scrambled siRNA/ATCOL complexes intravenously into 20-week-old LGMD1C mice at 0, 4, 7, and 14 days (Fig. 2A). Strikingly, we observed the enlargement of a number of skeletal muscles, including the lower limbs, masseters, and more in mice treated with Mst-siRNA/ATCOL (Fig. 2B). Since the changes in the lower limb muscles were the most pronounced, we used them for further analyses. Indeed, we also observed a significant increase in muscle fiber size at 3 weeks after the first administration in mice treated with Mst-siRNA/ATCOL (Fig. 2C).

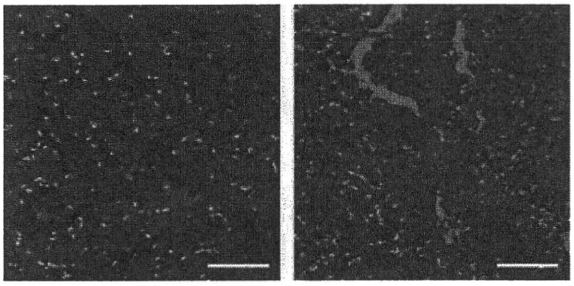

Fig. 1. Persistence and spread of an siRNA/atelocollagen (ATCOL, AteloGene Koken, Tokyo) complex following injection into the masseter muscle. A BLOCK-iT Alexa Fluor Red Fluorescent Oligo (10 μmol/L final concentration, Invitrogen) and ATCOL (100 μL) complex was injected into the masseter muscle of 20-week-old C57BL/6 mice. Gene expression from the BLOCK-iT Alexa Fluor Red Fluorescent Oligo/ATCOL complex injected in masseter muscle was assessed 2 weeks post-injection. Sections were examined following hematoxylin and eosin (H&E) staining (left) and serial section immunofluorescence to detect Alexa Fluor Red-positive cells (right). As expected, the Alexa Fluor Red Fluorescent Oligo expression was not evenly distributed across the tissue, and the majority of expression was located near the injection sites. Images were captured at 400× magnification. Scale bar, 100 μm.

These results indicated that intravenous administration of a myostatin-targeting siRNA with ATCOL specifically induced muscle hypertrophy in LGMD1C mice. The results were expressed as a ratio of the internal control and were analyzed statistically. Mst-siRNA/ATCOL-treated muscles (18.64 ± 4.18 μm) were significantly larger than control muscles (15.49 ± 3.12 μm) ($P < 0.0001$, $n = 100$). Histometric analysis showed that the myofibril sizes of quadriceps muscles treated with the Mst-siRNA/ATCOL complex were significantly larger than those of control quadriceps muscles (Fig. 2C,D). Examination of the sizes of 100 myofibers from each group showed that the Mst-siRNA/ATCOL-treated myofibril population exhibited a shift from smaller to larger sized fibers; the average myofibril size for Mst-siRNA/ATCOL-treated muscle was increased

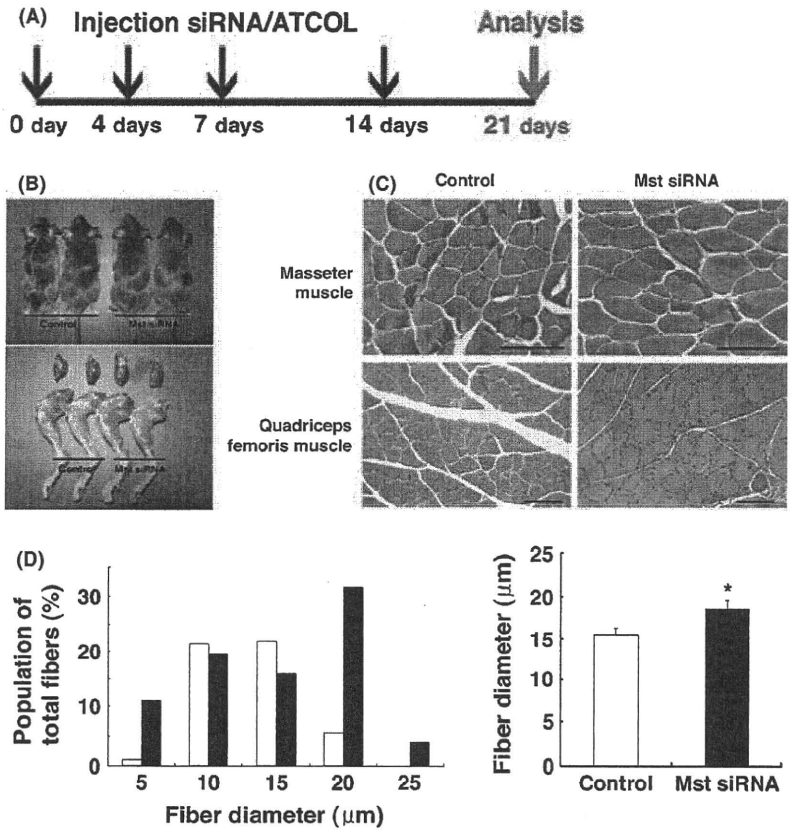

Fig. 2. Systemic administration of the Mst-siRNA/ATCOL complex led to increased skeletal muscle mass and fiber size in LGMD1C mice via inhibition of myostatin expression. In the experiments depicted in (A–C), Mst-siRNA (40 μmol/L final concentration) was mixed with ATCOL according to the manufacturer's instructions. (A) Time course analysis. Twenty-week-old male or female LGMD1C mice were anesthetized with Nembutal (25 mg/kg i.p.), and the Mst-siRNA/ATCOL complex (40 μmol/L in a 200 μL volume) was introduced intravenously via orbital veins at 0, 4, 7, and 14 days (n = 3). As a negative control, scrambled siRNAs were injected into LGMD1C mice. At 3 weeks after the first administration, the quadriceps muscles on both sides were harvested and processed for analysis. (B) Photographs of mice (upper panels) and lower limbs (lower panels). An increase in muscle mass was observed in the Mst-siRNA/ATCOL-treated (right), but not in control mice (left). (C) H&E staining of control (left) and Mst-siRNA/ATCOL-treated (right) masseter or quadriceps femoris muscle. Images of the masseter and quadriceps femoris were captured at 400× and 200×, respectively. Scale bar, 50 μm. (D) Distribution of the myofibril sizes of control (white bars) and Mst-siRNA/ATCOL-treated (black bars) quadriceps muscles. The right panel shows the average myofibril size (15.49 ± 3.12 μm vs. 18.64 ± 4.18 μm, respectively; n = 100; $P < 0.01$). The graphical representation of the data uses the following convention: mean ± SD. Mst-siRNA/ATCOL-treated muscles and mice are shown in black; control muscles and mice are shown in white. National Institute of Health (NIH) Image (NIH) software was used for morphometric measurements.

by approximately 1.2-fold relative to control muscle (Fig. 2D).

Hypertrophied Mst-siRNA/ATCOL-treated LGMD1C muscle fibers exhibit significantly improved contractile force generation

First, we tested the grip strength of mice before and after treatment. There were no statistically significant differences in the grip strength before and after treatment (Fig. 3D). We also evaluated the contractile properties of Mst-siRNA/ATCOL-treated LGMD1C muscle (Fig. 3C). We did not identify any statistically significant differences in the wet weights of Mst-siRNA/ATCOL-treated and untreated LGMD1C muscle. Unexpectedly, the specific force of untreated LGMD1C muscle was much lower than that of Mst-siRNA/ATCOL-treated LGMD1C muscle (Fig. 3A,B). We analyzed the specific force generated by tetanic stimulation (150 Hz) of TA muscles from LGMD1C mice treated with ATCOL-based control scrambled siRNAs or Mst-siRNA (0.568 ± 0.293 vs. 0.041 ± 0.351 N/cm^2, respectively; n = 4; $P < 0.05$).

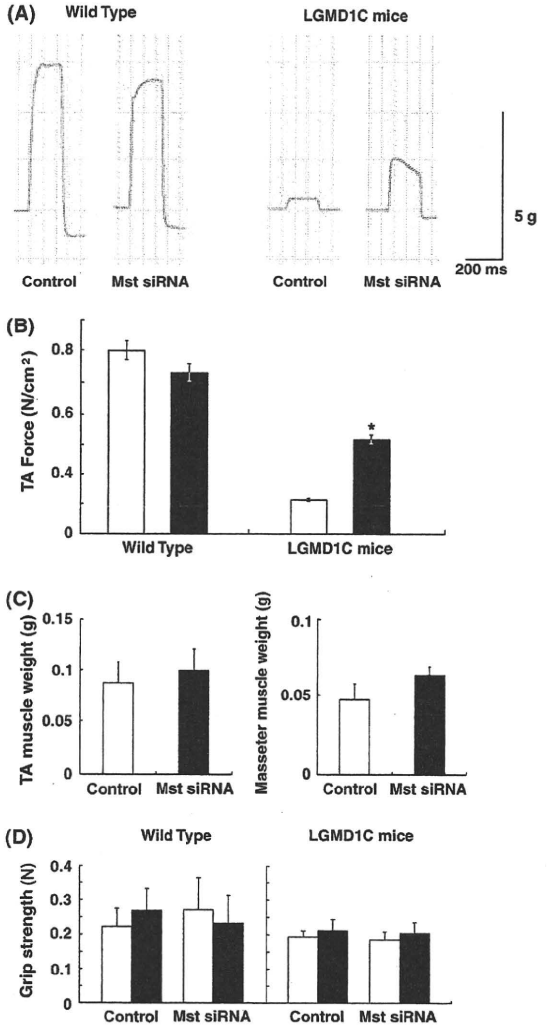

Fig. 3. Mst-siRNA/ATCOL-treated fibers exhibited significantly improved contractile force generation. (A) Specific force generated by tetanic stimulation (150 Hz) of TA muscles from wild-type or LGMD1C mice treated with ATCOL-based control scrambled siRNAs or Mst-siRNA. (B) The specific force of untreated LGMD1C muscle (□) was much lower than that of Mst-siRNA/ATCOL-treated LGMD1C muscle (■) (0.569 ± 0.293 N/cm^2 vs. 0.041 ± 0.351 N/cm^2, respectively; n = 4; $P < 0.05$). In contrast, in wild-type mice, the specific force was not different between untreated muscle and Mst-siRNA/ATCOL-treated muscle (0.888 ± 0.588 N/cm^2 vs. 0.925 ± 0.828 N/cm^2; n = 3. (C) There were no statistically significant differences in wet weights between untreated muscles and Mst-siRNA/ATCOL-treated muscles. (D) There were no statistically significant differences in grip strength between pre-treated mice (□) and after Mst-siRNA/ATCOL-treated mice (■).

Although wild-type fibers have been found to be hypertrophied (Kinouchi *et al.* 2008), the present results did not show a significant difference between the contractile force generated by Mst-siRNA/ATCOL-treated and untreated wild-type muscle (0.888 ± 0.588 vs. 0.925 ± 0.828 N/cm^2; n = 3). As shown in Figure 2D, histogram analysis demonstrated a shift to the right in the fiber distribution of Mst-siRNA/ATCOL-treated LGMD1C muscle relative to that of untreated LGMD1C muscle; larger caliber fibers were dominant, reflecting hypertrophy of Mst-siRNA/ATCOL-treated muscle fibers. Thus, hypertrophied Mst-siRNA/ATCOL-treated LGMD1C muscle fibers exhibited improved contractile force generation, but the increase in muscle weight did not correlate with increased force generation.

We previously reported that local and systemic administration of siRNA against myostatin coupled with ATCOL markedly stimulated muscle growth *in vivo* within a few weeks (Kinouchi *et al.* 2008), and that ATCOL-based gene therapy was associated with low immunogenicity. As expected, we did not observe any signs or symptoms suggestive of health problems during the experimental period of the current study.

Discussion

In the current study, we intravenously administrated a myostatin-targeting siRNA with ATCOL and analyzed the relationship between the extent of Mst-siRNA/ATCOL expression and the recovery of contractile force in LGMD1C muscles. Histogram analysis further demonstrated that the myofibril size distribution of Mst-siRNA/ATCOL-treated LGMD1C muscle fibers was shifted from smaller to larger sized fibers relative to control muscle fibers. We found that treatment of LGMD1C mice with the Mst-siRNA/ATCOL complex led to a significant increase in skeletal muscle mass and enhanced contractile force, similar to that reported previously with a myostatin blockade of dystrophic muscle (Bogdanovich *et al.* 2002).

There was no statistically significant difference in muscle weight between control and Mst-siRNA/ATCOL-treated muscles. It appeared that muscle weight did not correlate with force generation. Thus, hypertrophied Mst-siRNA-positive LGMD1C fibers seemed to greatly improve contractile force generation. Notably, the level of contractile force was dramatically improved by approximately 60% in Mst-siRNA/ATCOL-treated wild-type muscles relative to control muscles. Although the underlying molecular mechanisms by which Mst-siRNA/ATCOL treatment leads to increased contractile force remain to be determined, the current results are encouraging in that the function of caveolin-3-deficient muscles might be greatly improved. These findings are significant because the recovery of absolute maximal force and specific tetanic force are barometers of amelioration (Yoshimura *et al.* 2007).

To our knowledge, the results of the current study are the first to quantitatively and qualitatively demonstrate that *in vivo* myostatin siRNA gene transfer may serve as an effective treatment for muscular dystrophy. The potential benefit of myostatin siRNA gene therapy lies in the treatment of skeletal muscle waste in conditions such as muscular dystrophies (Bogdanovich *et al.* 2002), cachexia and HIV infection in advance of new therapies (Gonzalez-Cadavid & Bhasin 2004; Frimel *et al.* 2005). Although myostatin siRNA gene therapy would not correct the underlying pathophysiology of these diseases, it would counterbalance the effects by stimulating myofiber growth. The ease of administration of the myostatin-siRNA/ATCOL complex combined with its muscle-growth effect makes it a clinically valuable method of fighting against muscle atrophy. However, a strategy for the clinical use of this gene transfer method for human DMD patients requires further testing. Differences between humans and mice, including muscle size, life span and biological properties, should be taken into consideration (Yoshimura *et al.* 2007). In tumor-bearing mice, it was reported that ATCOL distributed siRNAs against luciferase to normal liver, lung, spleen and kidney tissues, as well as to bone-metastatic lesions (Takeshita *et al.* 2005). ATCOL was also reported to display low-toxicity and low-immunogenicity when it is transplanted *in vivo* (Ochiya *et al.* 2001; Sano *et al.* 2003).

Taken together, the results of the present study demonstrate that administration of siRNAs with ATCOL may be a promising therapeutic tool not only for muscular diseases, but also for other genetic diseases. The results of the current study indicate that treatment with Mst-siRNA/ATCOL led to an increase in muscle mass and functional recovery in the absence of obvious adverse effects in LGMD1C mice. The current study also provides evidence of ATOL-mediated delivery of siRNA to skeletal muscle. Therefore, ATCOL-mediated administration of siRNAs represents a powerful new tool for future therapeutic use in the treatment of diseases, including muscular atrophy.

Acknowledgments

We thank Nami Naoe, Masahiro Fujino and Tadashi Okada (Division of Neurology, Kawasaki Medical School) for expert technical assistance. This work was supported by an intramural research grant (20B-13) for neurological and psychiatric disorders of NCNP and a research grant (H20-018) for comprehensive research on disability, health and welfare from the Ministry of Health, Labour and Welfare, a Grant for Research on Psychiatric and Neurological Diseases and Mental Health from the Ministry of Health, Labour and Welfare of Japan (15131301) to Y.O, funding from JSPS KAKENHI (14370212) to YS and Research Project Grants from Kawasaki Medical School (15-115B and 16-601) to Y.O. and Y.S.

References

Bogdanovich, S., Krag, T. O., Barton, E. R., Morris, L. D., Whittemore, L. A., Ahima, R. S. & Khurana, T. S. 2002. Functional improvement of dystrophic muscle by myostatin blockade. *Nature* **420**, 418–421.

Bulfield, G., Siller, W. G., Wight, P. A. & Moore, K. J. 1984. X chromosome-linked muscular dystrophy (mdx) in the mouse. *Proc. Natl Acad. Sci. USA* **81**, 1189–1192.

Deconinck, N. & Dan, B. 2007. Pathophysiology of duchenne muscular dystrophy: current hypotheses. *Pediatr. Neurol.* **36**, 1–7.

de Fougerolles, A., Vornlocher, H. P., Maraganore, J. & Lieberman, J. 2007. Interfering with disease: a progress report on siRNA-based therapeutics. *Nat. Rev. Drug. Discov.* **6**, 443–453.

Elbashir, S. M., Harborth, J., Lendeckel, W., Yalcin, A., Weber, K. & Tuschl, T. 2001. Duplexes of 21-nucleotide RNAs mediate RNA interference in cultured mammalian cells. *Nature* **411**, 494–498.

Fire, A., Xu, S., Montgomery, M. K., Kostas, S. A., Driver, S. E. & Mello, C. C. 1998. Potent and specific genetic interference by double-stranded RNA in Caenorhabditis elegans. *Nature* **391**, 806–811.

Frimel, T. N., Kapadia, F., Gaidosh, G. S., Li, Y., Walter, G. A. & Vandenborne, K. 2005. A model of muscle atrophy using cast immobilization in mice. *Muscle Nerve* **32**, 672–674.

Gonzalez-Cadavid, N. F. & Bhasin, S. 2004. Role of myostatin in metabolism. *Curr. Opin. Clin. Nutr. Metab. Care* **7**, 451–457.

Kinouchi, N., Ohsawa, Y., Ishimaru, N., Ohuchi, H., Sunada, Y., Hayashi, Y., Tanimoto, Y., Moriyama, K. & Noji, S. 2008. Atelocollagen-mediated local and systemic administrations of myostatin-targeting siRNA increase skeletal muscle mass. *Gene Ther.* **15**, 1126–1130.

Magee, T. R., Artaza, J. N., Ferrini, M. G., Vernet, D., Zuniga, F. I., Cantini, L., Reisz-Porszasz, S., Rajfer, J. & Gonzalez-Cadavid, N. F. 2006. Myostatin short interfering hairpin RNA gene transfer increases skeletal muscle mass. *J. Gene Med.* **8**, 1171–1181.

McPherron, A. C., Lawler, A. M. & Lee, S. J. 1997. Regulation of skeletal muscle mass in mice by a new TGF-beta superfamily member. *Nature* **387**, 83–90.

Minakuchi, Y., Takeshita, F., Kosaka, N., Sasaki, H., Yamamoto, Y., Kouno, M., Honma, K., Nagahara, S., Hanai, K., Sano, A., Kato, T., Terada, M. & Ochiya, T. 2004. Atelocollagen-mediated synthetic small interfering RNA delivery for effective gene silencing in vitro and in vivo. *Nucleic Acids Res.* **32**, e109.

Nishi, M., Yasue, A., Nishimatu, S., Nohno, T., Yamaoka, T., Itakura, M., Moriyama, K., Ohuchi, H. & Noji, S. 2002. A missense mutant myostatin causes hyperplasia without hypertrophy in the mouse muscle. *Biochem. Biophys. Res. Commun.* **293**, 247–251.

Ochiya, T., Nagahara, S., Sano, A., Itoh, H. & Terada, M. 2001. Biomaterials for gene delivery: atelocollagen-mediated controlled release of molecular medicines. *Curr. Gene Ther.* **1**, 31–52.

Ohsawa, Y., Hagiwara, H., Nakatani, M., Yasue, A., Moriyama, K., Murakami, T., Tsuchida, K., Noji, S. & Sunada, Y. 2006.

Muscular atrophy of caveolin-3-deficient mice is rescued by myostatin inhibition. *J. Clin. Invest.* **116**, 2924–2934.

Sano, A., Maeda, M., Nagahara, S., Ochiya, T., Honma, K., Itoh, H., Miyata, T. & Fujioka, K. 2003. Atelocollagen for protein and gene delivery. *Adv. Drug Deliv. Rev.* **55**, 1651–1677.

Sunada, Y., Ohi, H., Hase, A., Ohi, H., Hosono, T., Arata, S., Higuchi, S., Matsumura, K. & Shimizu, T. 2001. Transgenic mice expressing mutant caveolin-3 show severe myopathy associated with increased nNOS activity. *Hum. Mol. Genet.* **10**, 173–178.

Takeshita, F., Minakuchi, Y., Nagahara, S., Honma, K., Sasaki, H., Hirai, K., Teratani, T., Namatame, N., Yamamoto, Y., Hanai, K., Kato, T., Sano, A. & Ochiya, T. 2005. Efficient delivery of small interfering RNA to bone-metastatic tumors by using atelocollagen in vivo. *Proc. Natl Acad. Sci. USA* **102**, 12177–12182.

Takeshita, F. & Ochiya, T. 2006. Therapeutic potential of RNA interference against cancer. *Cancer Sci.* **97**, 689–696.

Yoshimura, M., Sakamoto, M., Ikemoto, M., Mochizuki, Y., Yuasa, K., Miyagoe-Suzuki, Y. & Takeda, S. 2007. AAV vector-mediated microdystrophin expression in a relatively small percentage of mdx myofibers improved the mdx phenotype. *Mol. Ther.* **15**, 320–329.

Zhu, X., Hadhazy, M., Wehling, M., Tidball, J. G. & McNally, E. M. 2000. Dominant Negative myostatin produces hypertrophy without hyperplasia in muscle. *FEBS Lett.* **474**, 71–75.

EXPERIMENTAL CELL RESEARCH 316 (2010) 3087–3092

available at www.sciencedirect.com

ScienceDirect

www.elsevier.com/locate/yexcr

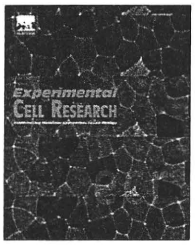

Review

Gene therapy for muscle disease

*Yuko Miyagoe-Suzuki, Shin'ichi Takeda**

Department of Molecular Therapy, National Institute of Neuroscience, National Center of Neurology and Psychiatry, 4-1-1 Ogawa-higashi, Kodaira, Tokyo 187-8502, Japan

ARTICLE INFORMATION

Article Chronology:
Received 25 March 2010
Revised version received 13 May 2010
Accepted 17 May 2010
Available online 24 May 2010

Keywords:
Dystrophin
Duchenne muscular dystrophy (DMD)
Recombinant adenoassociated viral (AAV)
Exon skipping
Antisense oligonucleotide
Gene therapy

ABSTRACT

The molecular mechanisms of Duchenne muscular dystrophy (DMD) have been extensively investigated since the discovery of the dystrophin gene in 1986. Nonetheless, there is currently no effective treatment for DMD. Recent reports, however, indicate that adenoassociated viral (AAV) vector-mediated transfer of a functional dystrophin cDNA into the affected muscle is a promising strategy. In addition, antisense-mediated exon skipping technology has been emerging as another promising approach to restore dystrophin expression in DMD muscle. Ongoing clinical trials show restoration of dystrophin in DMD patients without serious side effects. Here, we summarize the recent progress in gene therapy, with an emphasis on exon skipping for DMD.

Contents

* *Corresponding author.* Fax: +81 42 346 1750.
E-mail address: takeda@ncnp.go.jp (S. Takeda).

0014-4827/$ – see front matter © 2010 Elsevier Inc. All rights reserved.
doi:10.1016/j.yexcr.2010.05.022

Introduction

Muscular dystrophies are heterogeneous genetic disorders, characterized by progressive degeneration and weakness of the skeletal and cardiac muscles. DMD is severe and the most common type of muscular dystrophy; worldwide, approximately one in every 3500 boys born is afflicted with DMD.

The *DMD* gene is the largest known gene in humans, comprising over 79 exons, with a coding sequence of 11 kb and spans no less than 2.3 Mb of genomic DNA. DMD is caused by deletion (65%), duplication (15%), or nonsense and other small mutations (20%) in the *DMD* gene, all of which disrupt the open reading frame [1].

The *DMD* gene encodes dystrophin, which is located beneath the sarcolemma, assembles the dystrophin–glycoprotein complex at the sarcolemma, and links the internal cytoplasmic actin filament network and extracellular matrix, providing physical strength to muscle fibers [2]. At present, there is no effective therapy to stop the lethal progression of the disease, but several therapeutic approaches hold great potential. Here we focus on gene therapy for DMD and summarize AO-mediated exon skipping technology as a most promising therapy.

Adenoassociated virus -mediated gene therapy

Updates on rAAVs

The adenoassociated virus (AAV) is a tiny single-stranded, nonpathogenic, nonreplicative DNA virus belonging to the Parvovirus family. So far, more than 12 serotypes have been identified in primates [3]. Recombinant AAV (rAAV) is a powerful tool to deliver therapeutic genes to skeletal muscle [4–6]. Even in immunologically competent mice, the expression of the exogenous gene was shown to continue for years without evoking immune responses.

Importantly, rAAV has several serotypes that show tropisms to skeletal muscle. rAAV1 and rAAV2 are commonly used for direct delivery to skeletal muscle and mainly used in local treatment. rAAV-6 [7] plus the more recently developed rAAV-8 [8,9], and rAAV-9 [10–12] are powerful in systemic delivery of the therapeutic genes via the circulation to the musculature body-wide, including the diaphragm and heart.

Limited packaging size of rAAV

rAAV has a limitation in the length of the transgene it can accommodate (less than 5.0 kb). Full-length dystrophin, which is nearly 11 kb, cannot be incorporated into an AAV vector. To overcome this limitation, truncated but functional microdystrophins with a large deletion in the central rod domain have been constructed because studies of the genotype–phenotype relationships in DMD and Becker muscular dystrophy (BMD), a milder form of muscular dystrophy with near-normal life expectancy, have suggested that the rod domain has limited function and is largely dispensable [4]. Several types of microdystrophin were administrated to *mdx* mice locally [13] or systemically [7,14–16] and ameliorated pathology and improved muscle function. To expand the packaging capacity of the AAV vector, trans-splicing (ts) of two vectors and recombination of two overlapping (ov) rAAV vectors have been tested (reviewed in Trollet et al. [4]). A hybrid dual-vector system, which combines the features of the ts and ov vectors into a single system, has been reported to work well in skeletal muscle [17].

Immunity against rAAV in dog models

Based on the improvement of pathology and muscle function due to successful AAV-mediated gene transfer into dystrophic mice, preclinical studies using dystrophic dogs [18,19] and nonhuman primates [20,21] were performed. In dogs, considerable cellular immune response was often observed [18,19,22], and transient immune suppression was needed [23]. However, there is no clear explanation of why rAAVs evoke much stronger immune responses in dogs than mice.

Clinical trials

Immunity to AAVs is also a big concern in rAAV-mediated gene therapy for DMD. First, natural AAV infection is quite common in human populations, and preexisting antibodies could block AAV vector-mediated therapy. Second, after the first injection of rAAV vectors, the second injection is known to be much less effective due to a neutralizing antibody. Indeed, clinical trials using AAV vectors suggest that immune response to the vector and/or transgene product is the most important limitation of the rAAV-mediated gene therapy. To diminish a host immune response against the transgene product, utilization of a muscle-specific promoter active in both skeletal and cardiac muscles [24,25] is desirable. Codon optimization has also been demonstrated to be effective to reduce the virus titer [26]. A phase I/II clinical trial of intramuscular delivery of microdystrophin by AAV2.5-CMV-Mini-Dystrophin was initiated in 2006 (PI: JR Mendell; Trial ID: US-679; clinicaltrials.gov identifier: NCT00428935). More information can be obtained at http://www.wiley.co.uk/genetherapy/clinical/, http://www.clinicaltrials.gov, or http://www.mda.org.

Lentiviral vector-mediated gene transfer into muscle stem cells

Lentiviral vectors have a relatively large transgene carrying capacity (7.5–9 kb), integrate into the genomes of both dividing and nondividing cells, and achieve long-term transgene expression in a wide variety of tissues including skeletal muscle. Previously, lentiviral vectors have been used to introduce a mini-dystrophin gene into mouse skeletal muscle [27]. Because the expression levels of mini-dystrophin were low after direct injection of lentiviral

vectors into diseased muscle, this system seemed to be useful in modifying genetically autologous cells *ex vivo* rather than in direct injection *in vivo*. In fact, lentiviral vectors expressing mini-dystrophin transduced mouse satellite cells efficiently, and the transduced cells regenerated muscle fibers after transplantation [28]. Quenneville et al. [29] showed that lentiviral vectors are useful in transducing monkey muscle stem cells. The lentiviral vector has been recently used to modify muscle stem cells to deliver an antisense sequence linked to a modified U7 [30] or U1 [31] small nuclear RNA for restoration of the reading frame.

Antisense oligonucleotide (AO)-mediated exon skipping for *DMD* gene

Skipping of targeted exons

DMD is caused by mutations in the *DMD* gene that disrupt the open reading frame. BMD is also caused by mutations in the *DMD* gene, but in the case of BMD, the open reading frame is maintained. If we can skip (splice out) targeted exons by modification of splicing patterns and restore the reading frame, a shorter dystrophin protein can be restored in the DMD muscle, converting the DMD phenotype to a BMD phenotype. To this end, a number of antisense oligonucleotides (AOs) have been designed and tested *in vitro* [32–34] and *in vivo* [35–37]. Fig. 1 illustrates the skipping of exon 51 using one AO. Whether the resultant shortened dystrophin is functional or not depends largely on the function of the deleted part. In general, truncation of the rod domain is thought to be relatively harmless.

Single exon 51 skipping is expected to be suitable for approximately 13% of DMD patients. Multiple exon skipping is estimated to be applicable to more than 80% of DMD patients. Theoretically, the AO-mediated exon skipping strategy cannot treat patients with mutations in the promoter region, deletion of the first or last (79th) exon, deletion of the domain bound by dystroglycan: exons 62–69 [38] or large deletions (>35 exons) [39]. However, these mutations are rare, and the majority of patients have a mutation in the hotspot located between exons 43 and 55.

Design of AOs

AOs are designed to hybridize specific sequences, such as exon–intron boundaries, and exon splicing enhancer (ESE) sequences in transcripts. AOs interfere sterically with the splicing machinery [40,41]. There are several software programs, such as ESEfinder (http://rulai.cshl.edu/tools/ESE), to design antisense oligonucleotides, but extensive empirical analysis is still required for each exon.

AO chemistry, delivery in vivo, and toxicity

Among the AOs tested so far, AOs having a 2′-*O*-methyl phosphorothioate backbone (2′-*O*-MeAO) and phosphorodiamidate morpholino oligomers (PMOs) (Fig. 2) are commonly used in animal models and in clinical trials [42,43]. 2′-*O*-MeAOs have a chemically modified RNA structure (Fig. 2). The modifications increase the half-life and distribution to tissues. 2′-O-MeAOs have been well tolerated in clinical trials. PMOs have a morpholino backbone, are uncharged, are not recognized by cellular proteins, and, therefore, are rapidly cleared from plasma and excreted in urine. Very high doses of PMOs are reported to be well tolerated by animal models. This would be partly because PMOs hardly evoke innate immune responses.

In vivo delivery of AOs

One limitation of PMO-mediated exon-skipping therapy is that PMOs do not easily enter cardiac muscle. Recently, to improve the uptake of PMOs by cardiocytes, peptide-tagged PMOs (PPMOs) [44] and Octa-guanidine PMOs [45] were developed. These modified

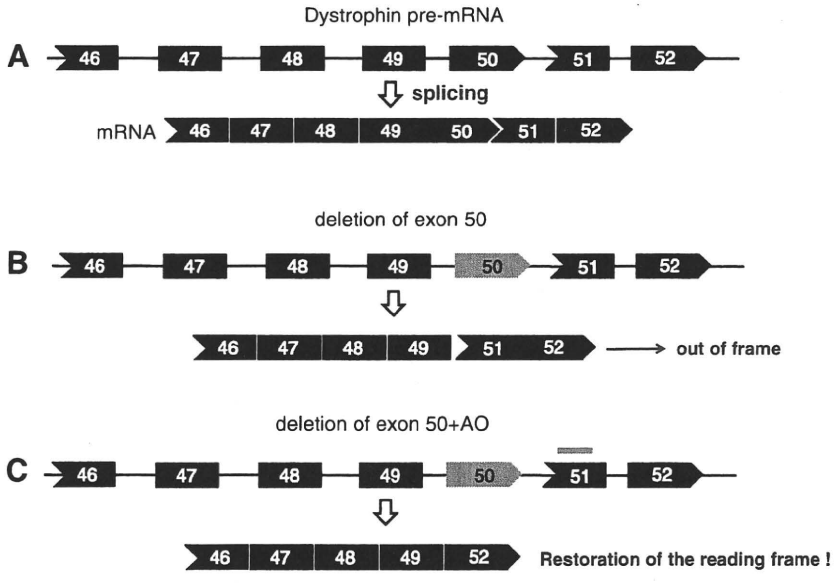

Fig. 1 – Exon skipping therapy for DMD patients with deletion of exon 51. (A) Normal dystrophin transcript and mRNA. (B) Deletion of exon 50 disrupts the open reading frame, leading to a premature stop codon, unstable mRNA, and a truncated protein. (C) Targeted skipping of exon 51 using AO restores the reading frame and produces a shorter but functional dystrophin that lacks exons 50 and 51. Blue bar indicates AO targeting the sequence in exon 51.